

POLITECNICO DI TORINO

Master's Degree in AUTOMOTIVE ENGINEERING



**Politecnico
di Torino**

Master's Degree Thesis

**Fuel economy assessment of
state-of-the-art energy management
strategies in different HEV architectures**

Supervisors

Prof. ANDREA TONOLI

PhD Candidate STEFANO FAVELLI

Candidate

HUAIZHI XUN

December 2023

Abstract

The Equivalent Consumption Minimization Strategy (ECMS) and Dynamic Programming (DP) are two different Energy Management Strategies for Hybrid Electric Vehicles (HEVs) powertrain control. Dynamic Programming is a backward approach that starts from the driving cycle itself, optimizing stage costs from the last system state to the first system state. Therefore, the solution of Dynamic Programming is generally used as a reference for establishing control rules, as the control trajectory derived from Dynamic Programming is not practically applicable but represents the optimal solution in theory. In this work, we use the Dynamic Programming algorithm to obtain the theoretical optimal control logic of hybrid IVECO DAILY, as a reference for the ECMS algorithm.

The application of the ECMS needs forward vehicle modeling and specifically a driver model to compare the actual vehicle speed and the speed profile in the driving cycle. Then ECMS generates commands to the vehicle system to fulfill the speed request and selects the optimal control logic with the lowest Equivalent Fuel Consumption at each time instant, which is associated to the Equivalence Factor that directly determines the utilization of the electric motor. The optimal Equivalence Factor varies with different conditions and, thereby, needs to be controlled. This thesis analyzes the fuel consumption and battery state of charge (SOC) fluctuation caused by 3 Equivalence Factor controllers (Relay-based switching logic, Adaptive-ECMS, and PID) over the WLTC and RDE driving cycles from a software perspective. In addition, the optimal control rule obtained from the Dynamic Programming algorithm is used as a comparative reference.

Apart from the Energy Management Strategies mentioned above, the performances of different HEV architectures (parallel and series-parallel) and various battery sizes are compared from a hardware point of view in this work.

Keywords: HEV architectures, Energy Management Strategies, Dynamic Programming, ECMS, Equivalence Factor, Battery, MATLAB, Simulink

Table of Contents

1	Introduction	1
1.1	Background	1
1.2	Motivation	2
1.3	Overview of the Project	3
1.4	Thesis Outline	4
2	Theoretical Background	6
2.1	HEV definition	6
2.1.1	HEV classification	6
2.1.2	HEV operating modes	7
2.1.3	HEV architectures	8
2.2	Energy Management Strategies of HEVs	9
2.2.1	EMS definition	9
2.2.2	EMS classification	9
2.3	Dynamic Programming (DP)	11
2.3.1	Dynamic Programming definition	11
2.3.2	Dynamic Programming Toolbox	12
2.4	Equivalent Consumption Minimization Strategy (ECMS)	13
2.4.1	ECMS definition	13
2.4.2	The effect of Equivalence Factor	13
2.4.3	The phase of ECMS implementation	14
2.5	Adaptive ECMS (A-ECMS)	14
2.5.1	SOC window and Equivalence Factor	14
2.5.2	Adaptive ECMS (A-ECMS) definition	15
2.5.3	Tuning of A-ECMS	15
3	Vehicle Modeling and Methodology	19
3.1	Vehicle parameters	19
3.1.1	Vehicle specifications	19
3.1.2	Vehicle Longitudinal Dynamics	20
3.1.3	Vehicle powertrain	21

3.1.4	Vehicle power split	23
3.2	Forward modeling approach with ECMS	24
3.3	Backward modeling approach with DP	25
3.4	Validation of the vehicle model	26
3.5	Usage of the vehicle model	27
3.6	Scope of Hybridization	29
3.7	Choice of HEV architectures	30
3.8	Battery sizing	31
4	Results & Discussion	32
4.1	P1 48V architecture in the WLTC Cycle	32
4.1.1	DP in WLTC driving cycle	32
4.1.2	DP vs. ECMS in WLTC driving cycle	34
4.2	P1 48V architecture in the RDE Urban Cycle	45
4.2.1	Comparison of power flows of ICE with DP and A-ECMS	46
4.2.2	Comparison of power flows of the electric motor with DP and A-ECMS	46
4.2.3	Comparison of SOC with DP and A-ECMS	46
4.2.4	Comparison of fuel consumption with DP and A-ECMS	48
4.2.5	Energy contribution and loss with A-ECMS	48
4.2.6	Available regenerative energy in A-ECMS algorithm	50
4.2.7	Summary of P1 48V architecture with DP and ECMS in the RDE Urban Cycle	50
4.3	P1 48V architecture in the RDE Rural Cycle	51
4.3.1	Comparison of power flows of ICE with DP and A-ECMS	52
4.3.2	Comparison of power flows of the electric motor with DP and A-ECMS	52
4.3.3	Comparison of SOC with DP and A-ECMS	52
4.3.4	Comparison of fuel consumption with DP and A-ECMS	53
4.3.5	Energy contribution and loss with A-ECMS	55
4.3.6	Available regenerative energy in A-ECMS algorithm	55
4.3.7	Summary of P1 48V architecture with DP and ECMS in the RDE Rural Cycle	56
4.4	P1 48V architecture in the RDE Motorway Cycle	57
4.4.1	Comparison of power flows and torque of ICE with DP and A-ECMS	57
4.4.2	Comparison of power flows and torque of the electric motor with DP and A-ECMS	58
4.4.3	Comparison of SOC with DP and A-ECMS	59
4.4.4	Comparison of fuel consumption with DP and A-ECMS	59
4.4.5	Energy contribution and loss with A-ECMS	61

4.4.6	Available regenerative energy in A-ECMS algorithm	61
4.4.7	Summary of P1 48V architecture with DP and ECMS in the RDE Motorway Cycle	62
4.5	P1 48V architecture vs. P2 200V architecture electric motor	63
4.5.1	P1 charge-sustaining vs. P2 charge-sustaining	64
4.5.2	P1 charge-sustaining vs. P2 charge-depleting	65
4.6	P1 48V architecture with different battery sizes	67
5	Summary of thesis and future works	69
5.1	Summary	69
5.2	Future works	71
	List of Tables	74
	List of Figures	76
	Bibliography	80

Chapter 1

Introduction

1.1 Background

As the automotive industry increasingly shifts towards environmentally friendly solutions, Hybrid Electric Vehicles (HEVs) have become a promising choice for reducing fuel consumption and emissions. The increasing market size of electric vehicles[1] is a strong reflection of electrification, as shown in Figure 1.1.

Compared to traditional vehicles, in addition to Internal Combustion Engines (ICE), HEVs have one or more electric motors[2], offering enhanced flexibility in energy provision. However, effectively allocating energy output from these sources is challenging. Due to the different efficiencies of ICE and electric motors at various torque and speeds, maintaining high efficiencies for both components under changing driving conditions becomes very intricate. Moreover, the limited battery capacity poses a challenge, as extremely low or high battery state of charge (SOC) can harm battery life. Thus, achieving optimal efficiency while managing SOC requires sophisticated powertrain control.

Furthermore, different HEV architectures and hardware specifications provide varied performance and costs. For instance, the P1 architecture, or parallel architecture, offers a simple yet efficient powertrain control structure. However, its flexibility is constrained due to the direct connection between the ICE and electric motors, resulting in less efficient ICE operations during acceleration since the ICE cannot be turned off. Conversely, the P2 architecture, with engaged clutches, provides a more flexible solution, mitigating some inefficiencies in the ICE but at the expense of increased complexity, raising costs and potentially affecting reliability. The absence of a standardized framework for selecting appropriate configurations for different HEVs persists because achieving a balanced compromise between performance and cost remains challenging in an objective manner.

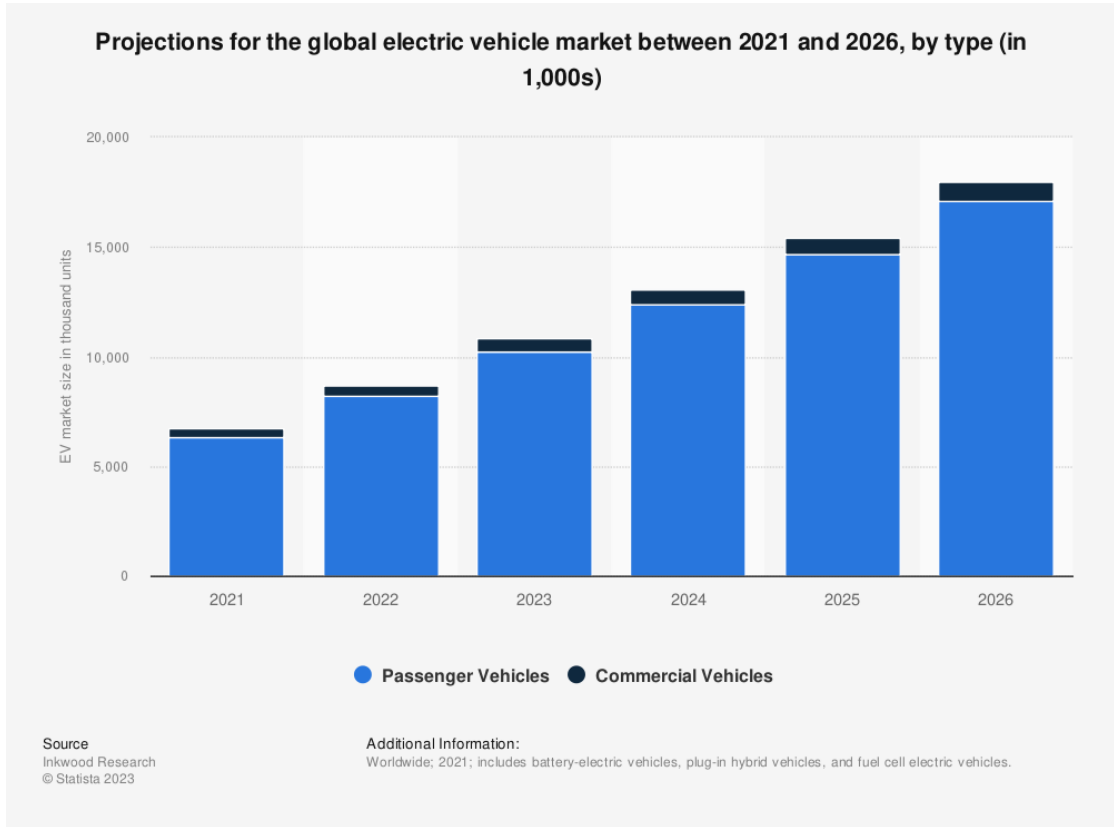


Figure 1.1: Global EV market projection between 2021 and 2026

1.2 Motivation

Although HEVs have been on the market for many years, the applicable optimal energy management strategy that can fully utilize the potential advantages of hybrid systems has not yet been invented.

The actual improvement of fuel economy in HEVs ranges from 10 percent for mild hybrid vehicles to over 30 percent for full hybrid vehicles[3]. This potential can only be achieved through complex control systems that optimize the internal energy flow of vehicles. It has been realized that using optimization strategies based on system models and effective objective functions to improve the effect of energy management is a way to achieve near-optimal results.

Therefore, this thesis will explore and compare two energy management strategies, the Equivalent Consumption Minimization Strategy (ECMS) and the Dynamic Programming (DP) algorithm, which have been widely applied in the analysis of HEV energy management, with a special focus on the Equivalence Factor controllers.

In addition, the choices of HEV architecture and battery size encounter many

dilemmas among performance, cost, and complexity, which need to be compromised considering different situations that are not merely from a technical point of view. This thesis will compare the performance of different HEV hardware in a quantitative approach.

1.3 Overview of the Project

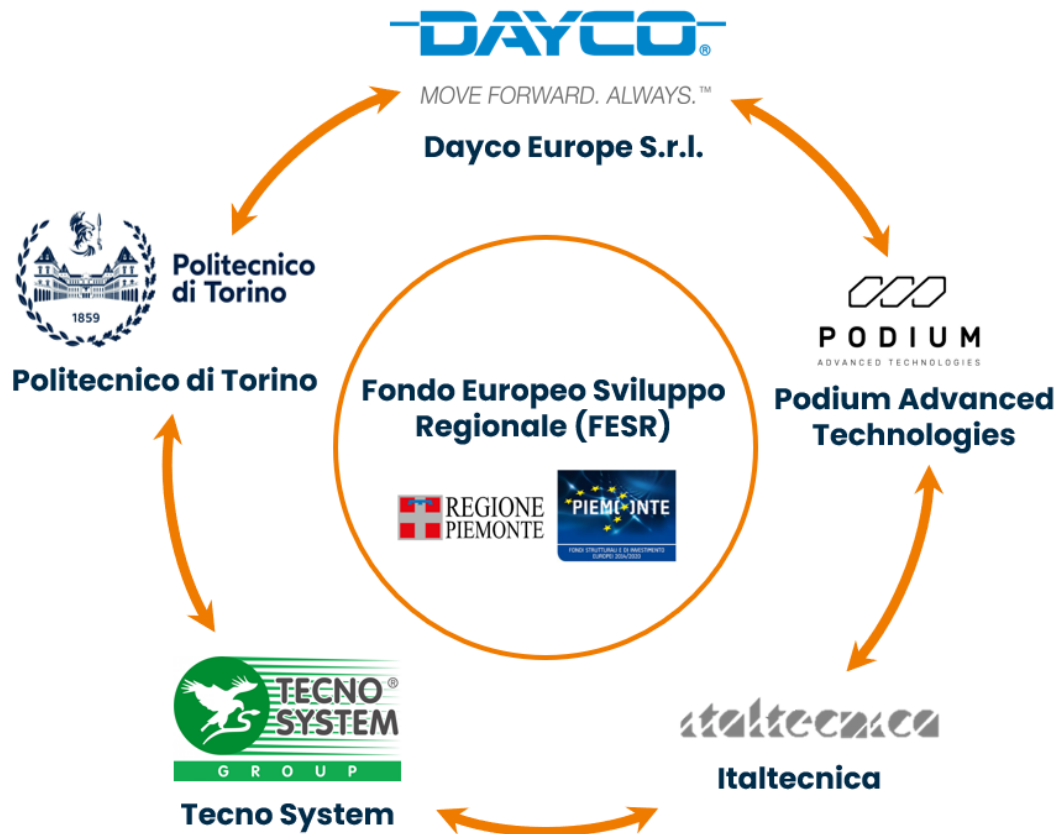


Figure 1.2: PITEF Project

The PITEF – AutoECO project is a government-funded research project supported by the Piedmont Region, where the PITEF is the abbreviation of Piattaforma Tecnologica di Filiera[4], translated as Supply Chain Technology Platform. The project aims to promote and validate an integrated system consisting of hybrid drive modules and control units on a demonstrator vehicle, which can evaluate potential benefits and utilize information provided by ADAS sensors in optimizing energy management control and improving energy efficiency. There are many

partners involved in this project, as shown in Figure 1.2. The road map consists of three steps:

- Step 1: Assess the benefits of fuel economy resulting from the integration of a P1 Hybrid Architecture.
- Step 2: Assess the further reduction potential brought about by the implementation of ADAS sensors.
- Step 3: Design, Integration, and Validation of Control Logic to optimize fuel consumption by utilizing the hybrid architecture and leveraging information from ADAS.

This thesis work is a part of the PITEF – AutoECO project, which investigates the performance of two HEV energy management algorithms, namely the ECMS and DP, in improving the fuel economy of IVECO DAILY (Figure 1.3), a P1 Hybrid light-duty vehicle. The simulation was conducted within the Worldwide Harmonized Light-Vehicle Test Cycle (WLTC) and Real Driving Emission (RDE) driving cycle by using MATLAB. This research builds a comparative analysis of these two algorithms in various driving scenarios, evaluating their impact on key parameters such as fuel consumption, battery state of charge (SOC), power flows, energy contribution, loss, etc. Moreover, the effects of different Equivalence Factor controllers (Relay-based switching logic, Adaptive-ECMS, and PID) in ECMS are also critical indicators for the feasibility of the implementation of ECMS in reality, because the optimal Equivalence Factor varies across different driving scenarios.

In addition to the energy management algorithms, the various architectures of HEV and different battery sizes are critical parts of optimization due to their different performance and cost, which will be discussed in detail in the following chapters.

1.4 Thesis Outline

This thesis is structured as follows:

- Chapter 2 presents the theoretical background of HEVs. Firstly, the definition of HEVs is summarized and the primary types and the architectures of HEVs are categorized. Then, the concept and the architecture of the Energy Management System (EMS) are outlined graphically. Afterward, the 2 Energy Management algorithms, ECMS and DP, which are the candidates for comparison, are introduced in detail.
- Chapter 3 focuses on the vehicle modeling process and model validation, employing both forward and backward approaches. The forward approach



Figure 1.3: IVECO DAILY

initiates with driver input, implementing the ECMS algorithm to control the power split between the ICE and the electric motor. Conversely, the backward approach originates from the driving cycle, using DP to work out the theoretically optimal results.

- Chapter 4 presents the results from the simulations covering three different Equivalence Factor controllers with the P1 48V architecture in different driving cycles, taking the results from DP as the reference. Furthermore, the results of different HEV architectures and battery sizes are computed by means of the DP algorithm.
- Chapter 5 is the final chapter, summarizing the results from the simulations carried out with various software and hardware configurations and indicating the possible future works that might be done afterward.

Chapter 2

Theoretical Background

Before discussing the simulation results, we will first introduce the definition and possible classification of Hybrid Electric Vehicles (HEVs) and provide the definition and classification of Energy Management Strategies (EMS). Then, the concepts of Equivalent Consumption Minimization Strategies (ECMS), Dynamic Programming (DP), and Adaptive ECMS (A-ECMS) are also summarized in this chapter. What is worth mentioning is that Adaptive ECMS involves the real-time adjustment of Equivalence Factors based on changing driving scenarios, ensuring a more responsive and adaptive energy management approach in HEVs. The construction and tuning processes of the A-ECMS controller will also be shown in this chapter.

2.1 HEV definition

Conventional vehicles are driven by an internal combustion engine through a transmission, which provides different transmission ratios, resulting in different wheel speeds. Hybrid vehicles combine two or more power sources to deliver power directly or indirectly. The primary energy source is usually the chemical energy in the fuel of internal combustion engines. “Hybrid” can refer to Hybrid Electric Vehicles (HEVs), mechanical hybrids, or fuel cell hybrids, depending on the category of secondary energy source.

In our research, the focus is on a Hybrid Electric Vehicle that incorporates an electric motor into the powertrain system, testing the fuel economy improvement due to the electrification.

2.1.1 HEV classification

The HEVs can be classified according to different involvements of the electric motor(s)[5], from Micro Hybrid to Plug-in Hybrid. A possible classification is as

follows:

- Micro Hybrid (start/stop): The start-stop systems allow the ICE to shut down and restart when the vehicle starts and stops frequently, especially in urban conditions, which reduces the engine idling time and therefore lowers fuel consumption and emission.
- Mild Hybrids (start/stop and kinetic energy recovery): The ICE in Mild HEV is coupled with an electric motor, usually in parallel. The electric motor can serve as a generator when the vehicle is braking, also known as regenerative braking. When the vehicle is coasting, braking, or stopping, the ICE is turned off. However, there is no purely electric mode in Mild HEVs.
- Full Hybrids (mild hybrid + electric launch + engine assist): The HEV having purely electric mode, pure ICE mode, and power-split mode between ICE and electric motor simultaneously can be categorized as Full HEV, which needs high-capacity battery pack for essential electric power to run the vehicle solely using the electric motor. In this case, the appropriate EMS is required to fully explore the potential of hybridized parts of vehicles, which will be discussed in the following.
- Plug-in Hybrids (full hybrid + electric range): The functionalities of Plug-in HEV (or PHEV) comprehensively cover those in Full HEV, but with rechargeable batteries that can be connected to external power and with a plug to connect to the electrical grid. Appropriate EMS is still needed, as Full HEV does.

In our baseline HEV configuration, the hybrid version of IVECO DAILY, the P1 48V architecture is a mild hybrid because it does not have a pure electric mode, as ICE has the same speed as the motor and cannot be shut down during vehicle acceleration, the ICE cannot charge the battery like the serial architecture either. On the contrary, another candidate for comparison, the P2 architecture 200V motor is a full hybrid, as the purely electric mode and the battery charging by the ICE can be realized by using planetary gear sets and clutches. However, the P2 architecture 200V motor is more complex than the P1 48V architecture. The detailed HEV operating mode and architecture and the comparison of P1 and P2 architecture will be discussed in the following.

2.1.2 HEV operating modes

Due to the assembly of electric motor(s), the vehicle might be possibly driven by ICE or electric motor(s), or both at the same time. There are three general

operating modes for HEVs, depending on the driving scenarios and the control logic of the energy management system:

- **Purely Electric Mode:** In this mode, the vehicle is propelled solely by the electric motor(s), with no contribution from the ICE. It relies entirely on the electrical energy for propulsion.
- **Pure ICE Mode:** Conversely, the Pure ICE mode indicates that the vehicle is exclusively powered by the ICE. In this mode, the electric motor remains inactive, and the vehicle's propulsion is driven solely by the ICE.
- **Power-split Mode:** The Power-split mode represents a hybrid state where the vehicle's power delivery is a combination of electric motors and ICE. These two power sources work together to drive the vehicle, and their contributions are synchronized to optimize performance and efficiency.

2.1.3 HEV architectures

The architectures of HEV can be classified according to the means of connection among ICE, electric motor(s), and drivetrain. A possible classification of HEV architectures is the following[6]:

- **Serial:** In the serial architecture, the ICE drives the generator, and the electrical energy generated by the generator can be added to the electrical energy of the Rechargeable Energy Storage System, and then transmitted to the electric motor to drive the wheels.
- **Parallel (P1: Figure 3.1):** The sum of power in the parallel architecture is only mechanical, where the ICE and electric motor(s) are connected through a gear set, chain, or belt to add up their torque and transmit it to the wheels.
- **Power-split:** The ICE and electric motor(s) are connected to a power-split device (usually a planetary gear set), and the power from the ICE and the electric motor(s) can be merged through both a mechanical and an electrical path, thus combining series and parallel operation.
- **Series/Parallel (P2: Figure 3.8):** In the Series/Parallel architecture, the engagement/disengagement of one or more clutches allows the powertrain configuration to be changed from series to parallel, and vice versa, thereby allowing the use of the most suitable configuration for the current operation.

Different HEV architectures have various flexibility, and high flexibility improves fuel economy. However, its complex structure can also have reliability issues

and high costs. Therefore, how to choose an appropriate HEV architecture is always an important issue, which depends on the market positioning of automotive products and the automotive culture of various regions, rather than just technical considerations.

2.2 Energy Management Strategies of HEVs

2.2.1 EMS definition

The control of HEVs[7] is composed of two tasks, as shown in Figure 2.1: One is the low-level control task, where the powertrain is controlled by classical feedback control methods. The second task is the high-level control (or supervisory control), which optimizes the power split between the primary and secondary sources of energy. This optimization is based on the power required by the vehicle, which meets the speed profile of the driving cycle while maintaining the battery state of charge (SOC) within a certain window to extend battery life.

The Energy Management Strategies (EMS) is used to complete the second task, the high-level control, receiving and processing information from the vehicle and driver, sending the optimal set point to the actuator and executing it by the low-level control layer, responsible for selecting the optimal modes of operation for the hybrid powertrain, which include start-stop, power-split, and electric launch.

2.2.2 EMS classification

The existing literature describes various categories of EMS, which can be generally categorized into two main groups: rule-based and model-based optimization methods[8][9][10], their detailed definitions are as follows:

Rule-based approaches

These approaches are recognized for their real-time effectiveness. They do not require explicit minimization or optimization but instead rely on a predefined set of rules to determine control variables at each time instant. These rules are usually developed based on heuristics, intuition[11], or knowledge gained from optimal global solutions obtained through mathematical models and optimization algorithms[12][13][14].

For example, the threshold of changing the purely electric mode to the pure ICE mode can be a certain engine speed or power requested by the driver, which is defined according to the experience or experimental results that can improve the fuel economy. Similarly, whether to use the power split mode or not can depend

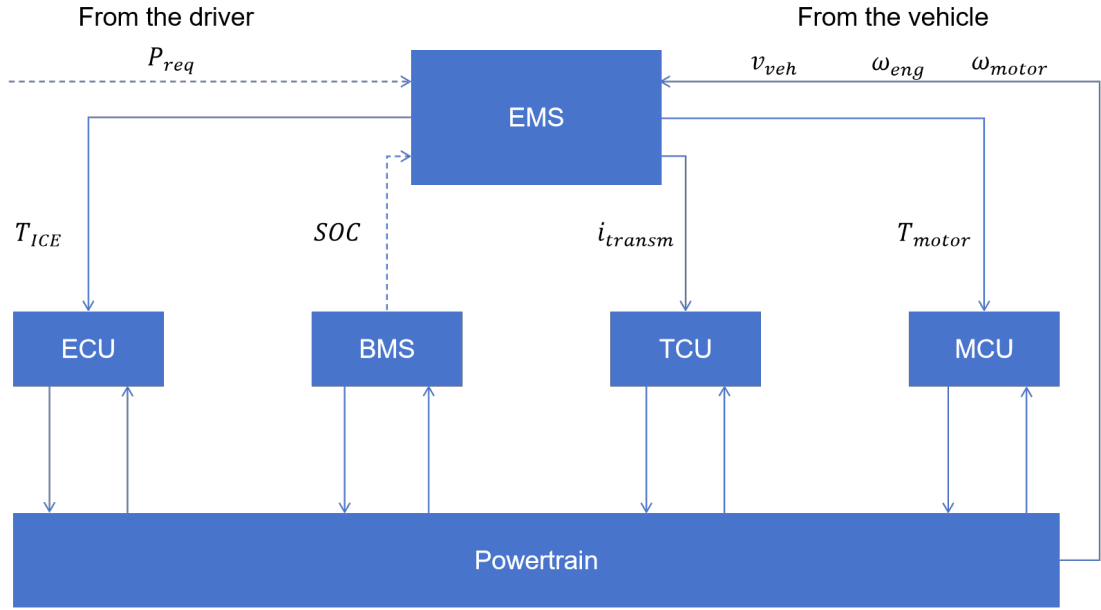


Figure 2.1: HEVs control tasks, where ECU is the Engine Control Unit, TCU is the Transmission Control Unit, BMS is the Battery Management System, and MCU is the Motor Control Unit

on the current battery state of charge (SOC) because we want to keep the SOC to the target value.

Model-based optimization

In the model-based strategies, the optimal actuator set-points are established by minimizing a cost function over a predefined and well-defined driving cycle. This approach leads to globally or locally optimal solutions. While model-based optimization control methods are often not directly suitable for real-time implementation due to their predictive nature and complexity of computation. These methods can be utilized to derive practical rules for online implementation or serve as reference benchmarks to assess the effectiveness of alternative control strategies.

Model-based optimization methods can be categorized into two main approaches, numerical and analytical:

- Numerical optimization methods (global optimum): In numerical optimization methods, such as Dynamic Programming (DP)[14] and Genetic Algorithms[15], the entire driving cycle is analyzed, and the global optimum is determined through numerical computations. These methods consider the complete driving cycle, accounting for all relevant parameters and constraints, and aim to

identify the optimal solution that minimizes or maximizes the objective function. Numerical optimization methods are particularly suitable for problems where analytical solutions are not feasible or efficient.

- Analytical optimization methods (local optimum): In contrast, analytical optimization methods use analytical equations to obtain solutions. In analytical methods, Pontryagin’s minimum principle[16] has special significance. The Equivalent Consumption Minimization Strategy (ECMS)[17] also belongs to this category, as it involves minimizing the instantaneous cost function for each time instant within the driving cycle. However, local optimization does not definitely result in global optimization, thus, local optimization is regarded as a sub-optimal solution.

2.3 Dynamic Programming (DP)

2.3.1 Dynamic Programming definition

Dynamic Programming (DP) was originally proposed by Richard Bellmann[18] in 1950 and has been widely applied in various fields. In the context of Hybrid Electric Vehicles (HEVs), DP plays a crucial role as an ideal optimal reference, especially in solving multi-stage decision-making problems with limited and deterministic constraints, such as gear number and battery state of charge (SOC) in a hybrid powertrain. Because HEVs integrate traditional ICE and electric motors, they require complex control strategies to optimize energy utilization, improve fuel efficiency, and reduce emissions.

In multi-stage decision-making problems, decisions are made across stages with the aim of minimizing the costs incurred. At each stage, the progress of the system is completely predictable, and given the state variables and control variables, the system’s state in the next stage can be predicted without any uncertainty.

Given the initial state of the system x_0 , the optimization problem lies in selecting the appropriate control variables over N stages (u_0, u_1, \dots, u_{N-1}) that minimize the total cost.

$$J(x_0, u_0, u_1, \dots, u_{N-1}) = F(x_N) + \sum_{k=0}^{N-1} L_K(x_k, u_k) \quad (2.1)$$

where x_k is the system state k , u_k is the control logic from state k to state $k+1$, $J(x_0, u_0, u_1, \dots, u_{N-1})$ is the total cost, $L_K(x_k, u_k)$ is the stage cost incurred by advancing one stage, and $F(x_N)$ is a terminal cost associated to the terminal system state.

The goal of the optimization problem is to find the optimal cost $V_0(x_0)$, which is the minimum total cost that can be incurred:

$$V_0(x_0) = \min_{u_k \in U_k(x_k), k=1, \dots, N-1} (F(x_N) + \sum_{k=0}^{N-1} L_k(x_k, u_k)) \quad (2.2)$$

and the control sequence that minimizes it:

$$u_0^*, \dots, u_{N-1}^* = \underset{u_k \in U_k(x_k), k=1, \dots, N-1}{\operatorname{argmin}} (F(x_N) + \sum_{k=0}^{N-1} L_k(x_k, u_k)) \quad (2.3)$$

$U_k(x_k)$ is the set of feasible control variables that can be selected at stage k.

Backward Phase of Dynamic Programming

Start by setting:

$$V_N(x_N) = F(x_N) \quad (2.4)$$

Set k = N - 1 and solve:

$$V_k(x_k) = \min_{u_k \in U_k(x_k)} (L_k(x_k, u_k) + V_{k+1}(f_k(x_k, u_k))) \quad (2.5)$$

Where $V_k(x_k)$ represents the minimum cost that can be incurred if the system must evolve from stage k to stage N under a given initial state x_k , it is also known as the cost-to-go.

Set k back by one stage and repeat the last step until $V_0(x_0)$ is obtained.

Forward Phase of Dynamic Programming

Start from k = 0, and evaluate

$$u_k^*(x_k) = \underset{u_k \in U_k(x_k)}{\operatorname{argmin}} (L_k(x_k, u_k) + V_{k+1}(f_k(x_k, u_k))) \quad (2.6)$$

Advance the simulation by updating the state variables

$$x_{k+1} = f(x_k, u_k^*(x_k)) \quad (2.7)$$

Advance k by one stage and repeat these two steps until the last stage.

2.3.2 Dynamic Programming Toolbox

The Dynamic Programming algorithm used for the vehicle model in this thesis relies on the "DynaProg" toolbox[19], developed in 2021 by Federico Miretti, Daniela Misul, and Ezio Spessa at Politecnico di Torino. For more detailed information, please refer to the MATLAB Add-On "DynaProg"[20].

2.4 Equivalent Consumption Minimization Strategy (ECMS)

2.4.1 ECMS definition

The Equivalent Consumption Minimization Strategy (ECMS)[21] is a local optimization method that aims to minimize instantaneous costs at each time instant, known as “sub-optimal”. The term “sub-optimal” indicates a local minimization in fuel consumption at each time step, which may not necessarily result in the optimal fuel consumption for the entire driving cycle. The sub-optimal fuel consumption is derived from the integral of the local minimization of Equivalent Fuel Consumption for each time instant, where the local optimization depends on the control logic and specific time instants. Equivalent fuel consumption, shown in Equation 2.8, includes the actual fuel consumption generated by internal combustion engines and the virtual fuel consumption generated by the operation of electric motors. In addition, the optimal control logic for each time instant is selected from available options, which are related to specific equivalent fuel consumption values. Globally, all the energy comes from fuel.

$$\dot{m}_{f,eqv} = \dot{m}_{fc} + s * \frac{P_{bat}}{LHV} \quad (2.8)$$

Where $\dot{m}_{f,eqv}$ is the Equivalent Fuel Consumption at each time instant, \dot{m}_{fc} is the actual fuel consumption due to the use of internal combustion engines, $s * \frac{P_{bat}}{LHV}$ is the virtual fuel consumption due to the use of electric motor, and "s" is the Equivalence Factor (or s-factor).

Since power is the derivative of energy, P_{bat} is related to $\dot{S}OC$, the Equivalent Fuel Consumption can be rewritten as Equation 2.9.

$$\dot{m}_{f,eqv} = \dot{m}_{fc} + \lambda * \dot{S}OC(t) \quad (2.9)$$

In this expression, the second term is from P_{bat} -related to $\dot{S}OC$ -related.

2.4.2 The effect of Equivalence Factor

The Equivalence Factor (or s-factor) has a significant impact on charging sustainability. The control logic prioritizes configurations with the lowest Equivalent Fuel Consumption. Consequently, lower s-factor will tend to use electric motors frequently, since the use of electric motors results in a lower Equivalent Fuel Consumption, which, however, may affect charging sustainability.

On the contrary, an excessively high s-factor will restrict the utilization of electric motors, leading to insufficient exploration of the potential of hybrid systems.

2.4.3 The phase of ECMS implementation

The general phase for the implementation of ECMS at each time instant is as follows:

- Power demand and powertrain state identification: Given the state of the system (required power, engine speed, electric motor speed, SOC, etc), the acceptable range of control values that satisfies the instantaneous constraints has to be identified.
- Identification of a finite number of control candidates: Discrete the interval of control variables into a finite number of control candidates.
- Equivalent fuel consumption computation: The Equivalent Fuel Consumption is computed for each control candidate.
- Optimal control value selection: select the control candidate that minimizes the Equivalent Fuel Consumption.

2.5 Adaptive ECMS (A-ECMS)

2.5.1 SOC window and Equivalence Factor

By carefully controlling the state of charge (SOC) of the battery within an appropriate window, the HEV system can efficiently optimize the power split between the electric motor and the ICE while extending the battery life.

While tuning the SOC window in the RDE Rural driving cycle, characterized by medium and high speeds with frequent acceleration and deceleration, we observed that the SOC window has a direct impact on fuel consumption. This effect is due to the direct relationship between the SOC window and the Equivalence Factor with a penalty function for SOC which directly influences the utilization of the electric motor, thereby exerting a notable influence on fuel consumption. Detailed data from these experiments are presented below.

The SOC window in the RDE Rural driving cycle, initially set between 0.55 and 0.65, has a target SOC value of 0.6 as recommended by the OEM. To optimize the SOC window, the first step involves maintaining the target SOC at 0.6 while changing the allowable range of SOC values. Table 2.1 provides the details of the tuning process.

The next step is to maintain the original SOC window and focus on changing the target SOC value. The details of this tuning process are presented in Table 2.2.

It can be observed that the SOC window and target SOC change the fuel consumption because they influence the Equivalence Factor that directly determines the usage of the electric motor. Thereby, the Equivalence Factor should be a function

Table 2.1: Tuning of SOC window

SOC window [%]	FC [L]	ΔSOC [%]	E_{Motion}	E_{ICE}	E_{Motor}	$E_{Regen.}$
[55, 65]	3.468	0.775	-7.566	12.343	0.715	-1.011
[56, 64]	3.488	4.009	-7.598	12.442	0.652	-0.978
[54, 66]	3.417	-3.361	-7.557	12.134	0.780	-1.039

Table 2.2: Tuning of target SOC

Target SOC [%]	FC [L]	ΔSOC [%]	E_{Motion}	E_{ICE}	E_{Motor}	$E_{Regen.}$
60	3.468	0.775	-7.566	12.343	0.715	-1.011
61	3.449	3.987	-7.574	12.275	0.694	-1.042
59	3.496	4.896	-7.567	12.482	0.685	-1.036

of SOC, aiming to maintain the SOC to the target value, when SOC is lower than the target SOC, the Equivalence Factor should be increased to hinder the use of the electric motor, when SOC is higher than the target SOC, the Equivalence factor needs to be decreased to promote the use of electric motor. So a controlling approach named "Adaptive ECMS" is invented to associate the Equivalence Factor and SOC.

2.5.2 Adaptive ECMS (A-ECMS) definition

By integrating all the information about SOC above, it can be concluded that the Equivalence Factor, which determines the battery utilization for the electric motor, should be a function of SOC. Thus, the Adaptive ECMS controller (Figure 2.2) is defined as Equation 2.10[21].

$$\lambda_{k+1} = \frac{1}{2}(\lambda_k + \lambda_{k-1}) + c_p(SOC_{ref} - SOC(t)) \quad (2.10)$$

Where the time instant $t = k \cdot T$, $k = 1, 2, \dots$, T is the time interval between the new value of the s-factor and the old one, λ_{k+1} is the new s-factor that will be used in the time interval $[kT, (k+1)T]$, λ is the current s-factor, λ_{k-1} is the previous s-factor, $SOC_{ref} - SOC(t)$ is the difference between the reference SOC and the actual SOC value, and c_p is the proportional gain of the feedback controller.

2.5.3 Tuning of A-ECMS

Tuning of proportional gain c_p in WLTC driving cycle

The tuning of the proportional gain c_p is rather sensitive and time-consuming, as shown in Table 2.3 and Figure 2.3. The proportional gain c_p is very small, if the

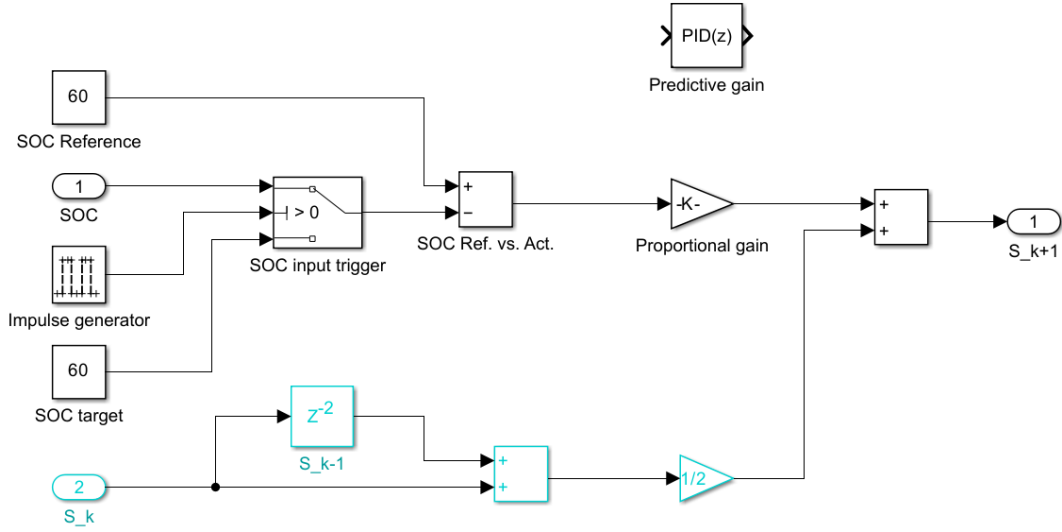


Figure 2.2: Adaptive ECMS controller architecture

gain is larger, the s-factor will go up and down strongly, while if the gain is too small, the controller will lose its ability to control the s-factor.

Table 2.3: Performance of different proportional gain c_p

c_p (T=5s)	0.00314	0.1	0.01	0.001
Fuel consumption [L]	2.329	2.347	2.377	2.332
SOC variation [%]	+0.654%	+1.364%	+0.581%	-0.156%

Tuning of the time interval for sampling in WLTC driving cycle

The strong sensitivity exists in the choice of the time interval for sampling, when the time interval is short, the s-factor will sharply fluctuate during the driving cycle, on the contrary, if the time interval is long, the effect of the controller will be impaired as well.

Tuning of the Initial s-factor in WLTC driving cycle

The lower initial s-factor of "1" prompts the control system to utilize the electric motor for power supply right from the beginning of the driving cycle. Then the battery will be charged when the battery state of charge (SOC) reaches the lower limit of the SOC window. On the flip side, when confronted with a higher s-factor of "2," the control system restrains the initial engagement of the electric motor.

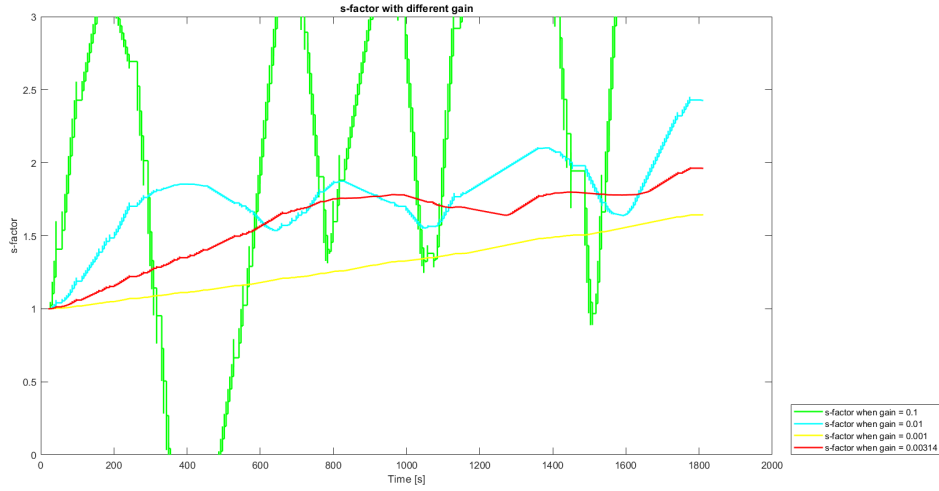


Figure 2.3: Tuning of proportional gain c_p

Table 2.4: Performance of different time intervals for sampling

T ($c_p=0.00314$)	5s	1s	10s	20s
Fuel consumption [L]	2.329	2.348	2.331	2.332
SOC variation [%]	+0.654%	+3.416%	+0.599%	-0.118%

This selection of the higher initial s-factor makes the battery charged at first, then discharged after the SOC reaches the upper limit of the SOC window. A graphical representation (Figure 2.5) demonstrating the SOC curves during the WLTC driving cycle under these different initial s-factors is presented below for a more intuitive understanding. The fuel consumption when using different s-factor are shown in Table 2.5.

In the final configuration, the proportional gain (c_p) and sampling time interval have been tuned through iterative trials, settling at 0.00314 and 5 seconds, respectively. It's important to note that due to the constrained time, the complete potential of the A-ECMS controller is rather likely not fully explored. This implies that further optimization and exploration of the architecture and parameters of A-ECMS might extract more advantages in fuel economy and battery life.

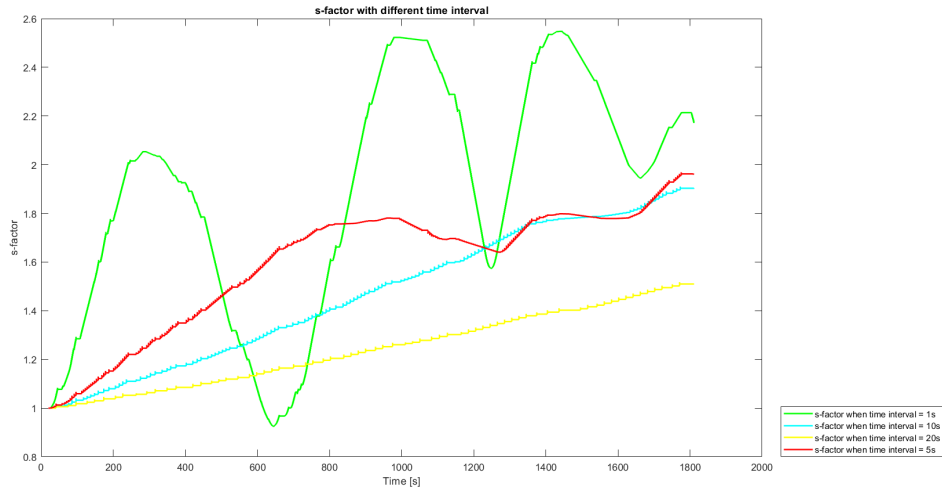


Figure 2.4: Tuning of time intervals for sampling

Table 2.5: Performance of different initial s-factor

Initial s-factor	1	2
Fuel consumption [L]	2.329	2.349

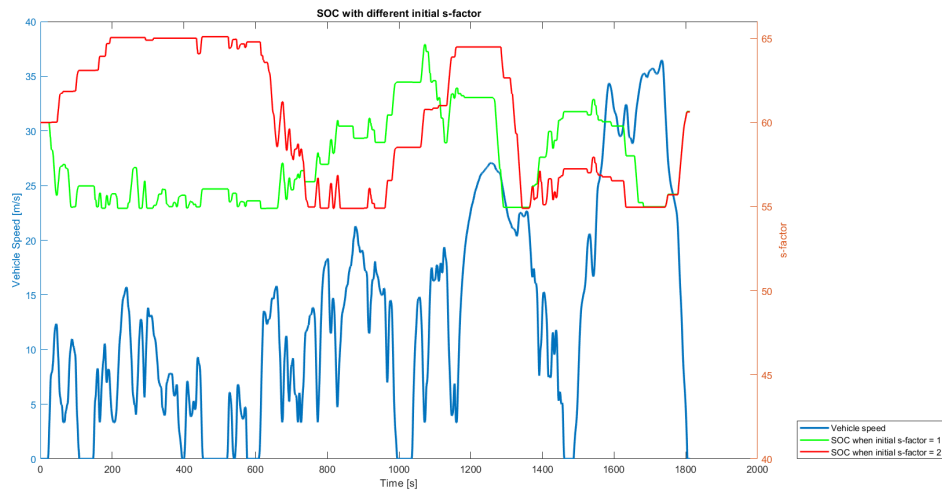


Figure 2.5: Tuning of initial s-factor

Chapter 3

Vehicle Modeling and Methodology

3.1 Vehicle parameters

3.1.1 Vehicle specifications

The subject of this study is IVECO DAILY, a lightweight vehicle with a diesel engine. The mean specifications of the vehicle are listed in Table 3.1. The main objective of this project is to evaluate the impact of electrification on vehicles, especially in terms of fuel consumption. The driving cycle analyzed in this thesis only considers the longitudinal dynamics of the vehicle.

Table 3.1: IVECO DAILY specification

Engine	FIA 2.3 Eu6d
Max Power	136 HP / 3250 rpm
Max Torque	350 Nm / 1500 rpm
Gearbox	Hi - Matic (ZF AT8)
Length	6087 mm
Width	2010 mm
Wheelbase	3520 mm
Height	2660 mm
Mass (empty)	2250 kg
Carrying Capacity	1250 kg

3.1.2 Vehicle Longitudinal Dynamics

The driving resistance exerted on the vehicle can be expressed in Equation 3.1, and the force acting on the vehicle is Equation 3.2.

$$F_{Resistance} = F_0 + F_1 * V_{veh} + F_2 * V_{veh}^2 \quad (3.1)$$

$$F_{veh} = F_{Resistance} + m_{veh} * a_{veh} \quad (3.2)$$

Where $F_{Resistance}$ is the driving resistance, F_0 is the constant road-load coefficient, representing the resistance a vehicle encounters when it is not in motion, such as friction, rolling resistance of the tire, and other constant resistances. F_1 is the linear road-load coefficient, accounting for forces that change linearly with the vehicle speed, such as rolling resistance or aerodynamic drag due to speed. F_2 is the quadratic road-load coefficient, referring to factors like aerodynamic drag at higher speeds or non-linear rolling resistance. F_{veh} is the force acting on the vehicle, m_{veh} is the vehicle mass, a_{veh} is the acceleration of the vehicle, and V_{veh} is the vehicle speed.

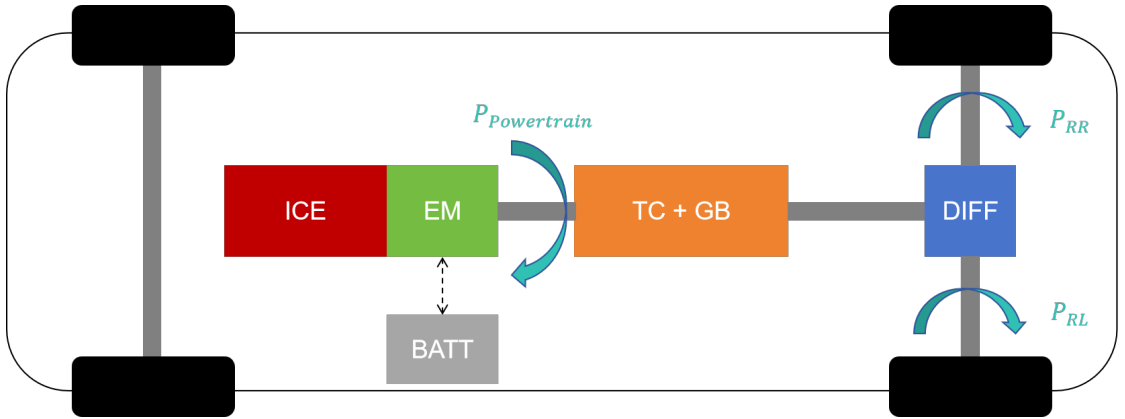


Figure 3.1: P1 architecture

In the baseline P1 48V HEV architecture (Figure 3.1), the ICE speed (ω_{ICE}) equals shaft speed (ω_{shaft}). And, the torque coupling ratio (τ_{tc}) is defined as the ratio between the speed of the electric motor (ω_{em}) and the speed of the shaft (ω_{shaft}). The torque coupling ratio (τ_{tc}) is equal to 1 in the P1 architecture because the electric motor speed equals the ICE speed, thus, equals the shaft speed.

However, the total torque transmitted to the shaft is the sum of the torque from the ICE and from the electric motor, respectively.

The relationship between the speed of the electric motor and the speed of the shaft is:

$$\omega_{em} = \omega_{shaft} * \tau_{tc} \quad (3.3)$$

The torque transmitted to the shaft by the electric motor is:

$$T_{shaft} = T_{em} * \tau_{tc} \quad (3.4)$$

The gear ratio (τ_{gb}) shows the relationship between the speed of the shaft and the speed of the final drive.

Crankshaft speed (rad/s):

$$\omega_{shaft} = \tau_{gb} * \omega_{fd} \quad (3.5)$$

The final drive ratio represents the relationship between the speed of the final drive and the speed of the wheel.

Final drive input speed (rad/s):

$$\omega_{fd} = \tau_{fd} * \omega_{wheel} \quad (3.6)$$

Final drive input torque (Nm):

$$T_{fd} = T_{wheel} / \tau_{fd} \quad (3.7)$$

Wheel speed (rad/s):

$$\omega_{wheel} = V_{vehicle} / R_{wheel} \quad (3.8)$$

Wheel torque (Nm):

$$T_{wheel} = F_{vehicle} / R_{wheel} \quad (3.9)$$

3.1.3 Vehicle powertrain

The engine performance is represented by a map composed of engine torque and engine speed, which is derived from real experiments. The different fuel flow rates and BSFC of the engine correspond to different engine speeds and torques, respectively. The fuel consumption is the integral of the fuel flow rate over time. Similarly, the performance of the electric motor is also map-based, which is obtained from real experiments as well. The engine maps will be illustrated in Chapter 4: Results & Discussion, while the efficiency of electric motors is very high compared to the ICE, so, as far as we are concerned, it is not essential to show the maps of electric motors.

As for the battery, in our simplified vehicle model (Figure 3.2), the battery model for the electric motor is composed of battery equivalent resistance and battery open circuit voltage.

The open circuit voltage and equivalent resistance of the baseline battery vary with the battery state of charge (SOC). The baseline 48V battery in this thesis comprises 14 cells arranged in series across two parallel branches, and its open circuit voltage and equivalent resistance are calculated based on the number and

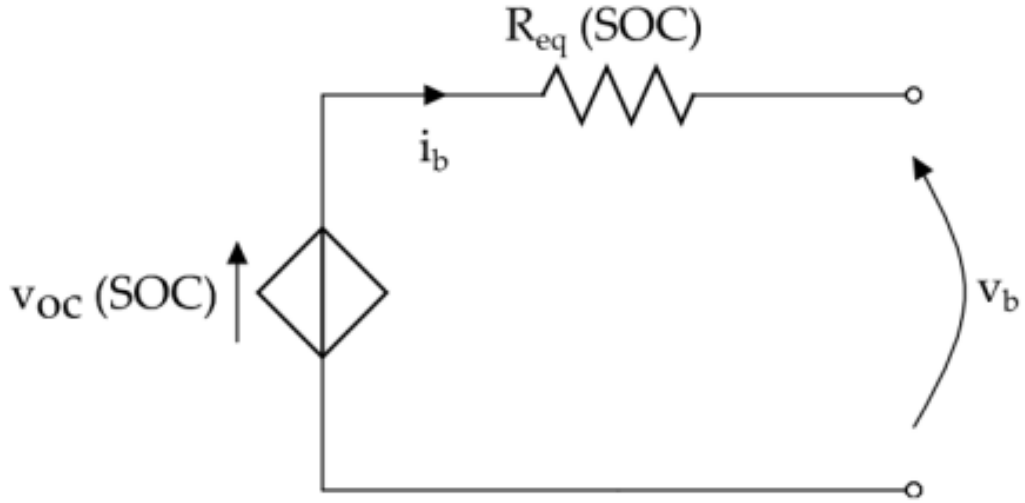


Figure 3.2: Simplified battery model

structure of cells. These specifications are determined based on the literature concerning the application of 48V batteries[22]. The characteristics of them are plotted in Figure 3.3.

The current of the battery (Equation 3.10) depends on the battery voltage, the battery resistance, and the power requested from the battery.

$$I_{batt} = \frac{V_{batt} - \sqrt{V_{batt}^2 - 4 * R_{batt} * P_{batt}}}{2 * P_{batt}} \quad (3.10)$$

The state of charge (SOC) of the battery in the next time instant (Equation 3.11) depends on the current SOC, battery current, Coulombic efficiency, and battery nominal capacity.

$$SOC_{next} = -\frac{\eta_{coul} * I_{batt}}{C_{batt} * 3600} * dt + SOC \quad (3.11)$$

When describing batteries, the discharge current is generally standardized using the C-rate[23], a common practice to explain differences in battery capacity. The C-rate is a measure of the discharge rate relative to the maximum capacity of a battery. Specifically, the rate of 1C indicates that the discharge current will

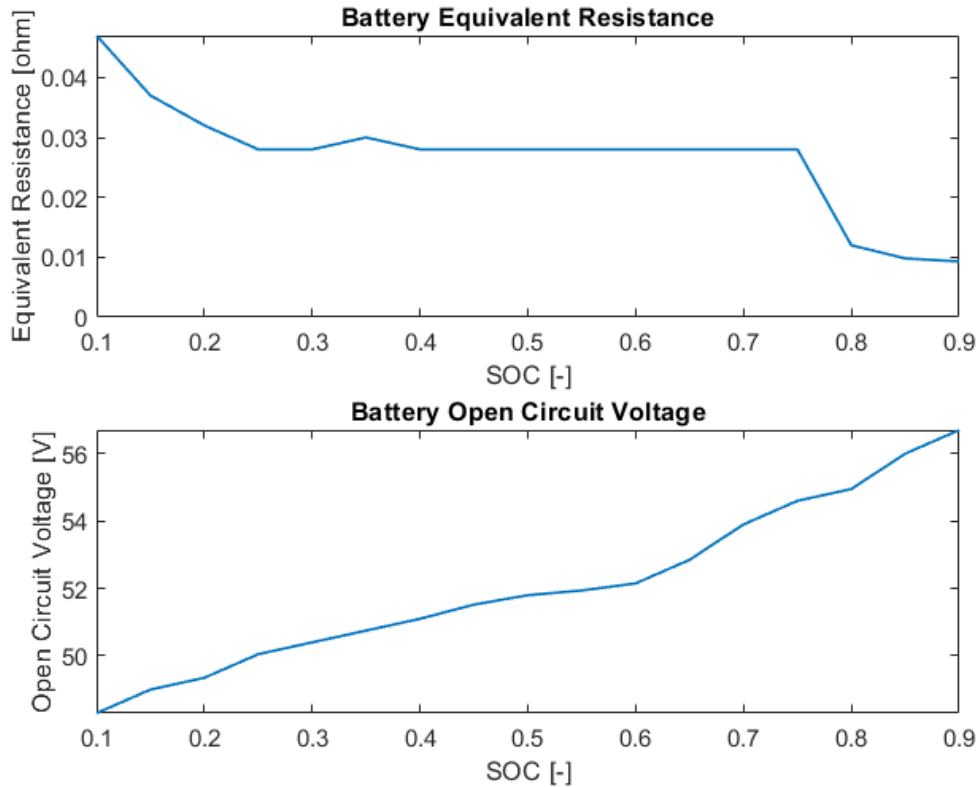


Figure 3.3: Battery specification

consume the entire battery within 1 hour. For consistency and security reasons, this thesis adopts the 10C ratio as the standard.

3.1.4 Vehicle power split

Now that the hybrid version of the IVECO DAILY incorporates an electric motor into its powertrain, the power-split factor (α_{eng}) is the ratio between the engine's power (P_{eng}) and the vehicle's required power (P_{req}). When the power-split factor is 1, the vehicle operates solely in ICE mode. Conversely, when the factor is 0, the vehicle operates in pure electric mode. When the power-split factor falls between 1 and 0, a power-split mode between the ICE and the electric motor (P_{em}) is engaged.

In the baseline P1 48V architecture, the ICE has the same speed as the electric motor, so the ICE cannot be completely shut down when the vehicle is propelled by the powertrain because of the physical characteristics of the engine operation. Thus, there is no purely electric mode in the P1 48V architecture.

Power-split:

$$p_{eng} = \alpha_{eng} * P_{req} \quad (3.12)$$

Power provided by electric motor:

$$p_{em} = (1 - \alpha_{eng}) * P_{req} \quad (3.13)$$

Power of ICE and electric motor:

$$P = T * \omega \quad (3.14)$$

Where P is the power of ICE or electric motor, T is the torque of ICE or electric motor, and ω is the speed of ICE or electric motor.

Energy delivered by ICE or electric motor:

$$E = \int_0^t P(t)dt \quad (3.15)$$

Where P is the power of ICE or electric motor and E is the energy of ICE or electric motor.

3.2 Forward modeling approach with ECMS

If a vehicle can be regarded as a mass point interacting with the external environment, its equation of motion from equilibrium can be written as Equation 3.16:

$$M_{veh} \frac{dv_{veh}}{dt} = F_{inertia} = F_{traction} - F_{roll} - F_{aero} - F_{grade} \quad (3.16)$$

Where M_{veh} is the effective vehicle mass, v_{veh} is the vehicle velocity in the longitudinal direction, $F_{inertia}$ is the inertia force of the vehicle, $F_{traction} = F_{powertrain} - F_{brake}$ is the traction force, F_{roll} is the rolling resistance (friction due to tire deformation and losses), F_{aero} is the aerodynamic resistance and F_{grade} is the force due to road slope.

The vehicle acceleration $\frac{dv_{veh}}{dt}$ is calculated as the result of the traction force generated by the powertrain, and then the speed is obtained by integrating the acceleration. This is the forward approach, which reproduces the physical causal relationship of the system, as shown in Figure 3.4.

The forward approach is a commonly chosen option in most simulators, as shown in Figure 3.4. For example, in the case of a hybrid vehicle forward simulator, the expected speed is compared to the actual vehicle speed, and a driver model (such as a PID controller) is used to generate braking or throttle commands to follow the driving cycle. This driver command is input to the supervisor block, which

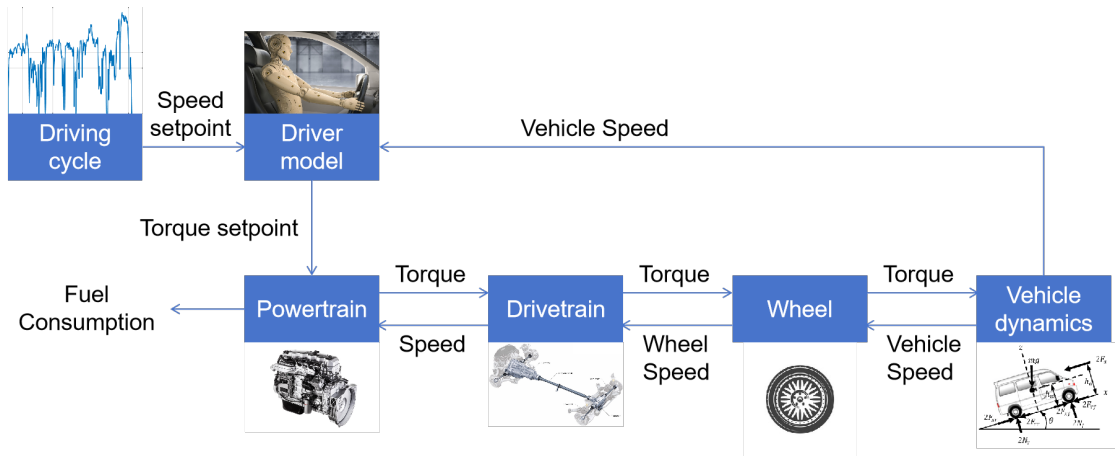


Figure 3.4: Forward modeling approach

is responsible for issuing the actuator settings (engine, electric motor, and brake torque) to the remaining components of the powertrain that ultimately generate traction and fuel consumption. Finally, the force is applied to the vehicle dynamics model, where the acceleration is determined by the equation of motion while taking into account road load information. Then, the new vehicle speed resulting from the acceleration generated by the powertrain is compared to the speed profile in the driving cycle again by the driver model, the same process repeats until the end of the driving cycle.

3.3 Backward modeling approach with DP

On the other hand, in order to calculate the traction force that is needed to be produced by the powertrain to fulfill the given acceleration, the equation of motion can be rearranged to Equation 3.17:

$$F_{traction} = F_{powertrain} - F_{brake} = F_{inertia} + F_{grade} + F_{roll} + F_{aero} \quad (3.17)$$

The force follows the velocity profile of the driving cycle and the traction force is calculated starting from the inertia force: in this case, it is assumed that the vehicle is following a prescribed velocity and acceleration profile, and $F_{traction}$ represents the corresponding force that the powertrain must supply.

In contrast with the forward modeling approach, the backward simulator (Figure 3.5) operates without a driver model, which utilizes the requested speed as input, while engine torque and fuel consumption are the outputs. The simulator calculates the net traction force required based on factors such as speed, payload, slope, and

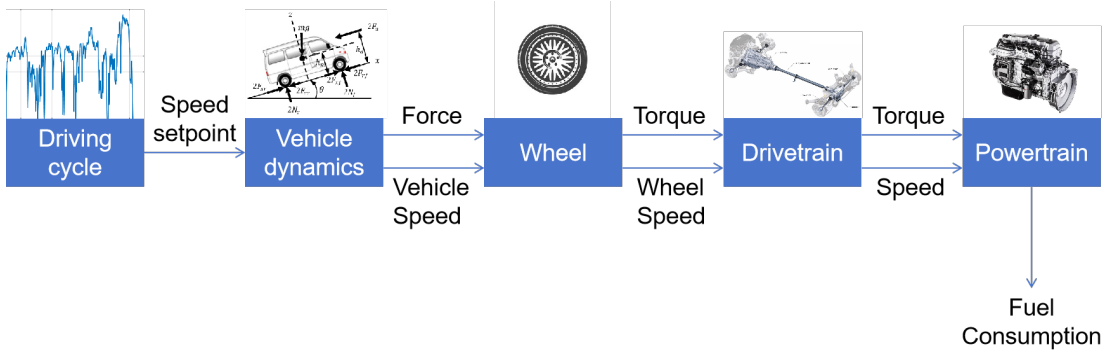


Figure 3.5: Backward modeling approach

vehicle attributes. Using these data, the simulator determines the torque that should be delivered by the powertrain. Subsequently, the torque and speed characteristics of different powertrain components are taken into account to establish engine operating conditions, thereby determining the fuel consumption.

3.4 Validation of the vehicle model

Table 3.3 compares the fuel consumption of the forward model (with ECMS), backward model (with DP), CARS-AVL TestBed, and FEV Roller during the WLTC driving cycle. According to the mean value of the results in the real experiments, the mismatch of the forward model on WLTC is less than 2.5%, of the backward model is around 4% to 6%, as Table 3.4 shows. It should be noted that the backward model also selects high gears at low speeds (shown in Figure 3.7), which theoretically reduces fuel consumption, but is not realistic in practice.

Table 3.2: Coast-down values in Model Validation

Vehicle mass	3283 kg
F0	345 N
F1	0 N/(km/h)
F2	0.1007 N/(km/h) ²

Figure 3.6 compares the engine operating points for ECMS, DP, and Real Experiment in Pure ICE mode during the WLTC driving cycle, revealing that DP (purple) leads to a distribution of engine operating points that is closer to the OOL compared to ECMS, with lower average engine speeds. ECMS (blue) makes the engine operate at higher average speeds and similar torque compared to DP. The average engine speed in the Real Experiment is lower than that in ECMS but

Table 3.3: ICE-only results - WLTC

Test platform	FC [L]	Distance [Km]	FC [L/100Km]
CARS-AVL TestBed	2.710	23.302	11.623
FEV Roller	2.784	23.363	11.916
Forward model	2.762	23.197	11.905
Backward model	2.599	23.283	11.162

Table 3.4: Model mismatch - WLTC

Numerical results	FEV	CARS
Forward model mismatch on WLTC	-0.092%	+2.426%
Backward model mismatch on WLTC	-6.328%	-3.966%

higher than that in DP, as the yellow points show.

Figure 3.7 compares the gear shifting among DP, ECMS, and Real Experiment, with Pure ICE mode during the WLTC driving cycle. DP exhibits the highest gear number, resulting in lower engine speed as the engine map shows. The gear numbers in Real Experiments are slightly lower than those in DP, especially at low-speed regions. Lastly, The ECMS, however, with Pure ICE mode, has the lowest average gear number, which is consistent with the engine operating points observed in the engine map.

The Table 3.5 and Table 3.6 compare the fuel consumption of the forward model, CARS-AVL TestBed, and FEV Roller during the RDE driving cycle. The mismatch between the results of the forward model and the real vehicle is less than 7.5%. While, the results of the backward model are not comparable with others in the RDE driving cycle because they are down-sized due to limited vehicle performance.

Table 3.5: ICE-only results - RDE

Test platform	FC [L]	Distance [Km]	FC [L/100Km]
CARS-AVL TestBed	12.336	83.212	14.825
FEV Roller	11.745	83.928	13.995
Forward model	11.266	84.065	13.716
Backward model	-	-	-

3.5 Usage of the vehicle model

The forward and the backward modeling approaches have different utilities apart from their different modeling process. In brief, the solution derived from the

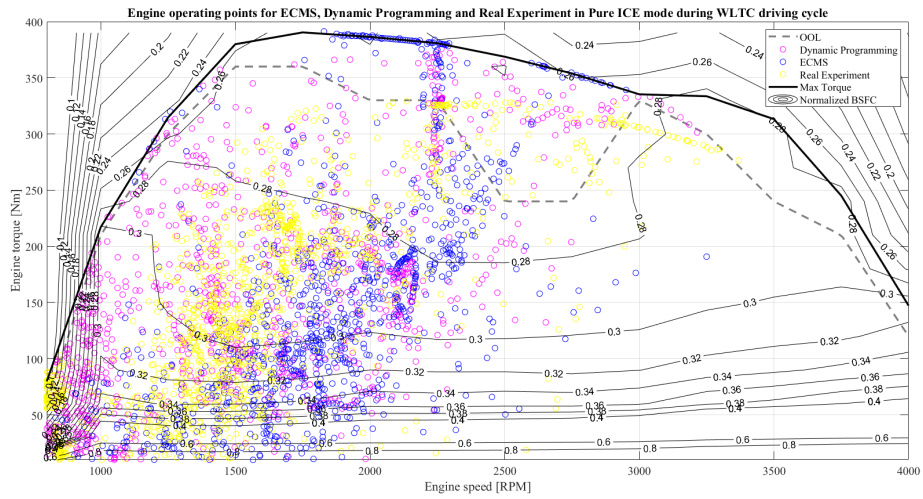


Figure 3.6: Engine operating points for ECMS, DP, and Real Experiment in Pure ICE mode during WLTC driving cycle

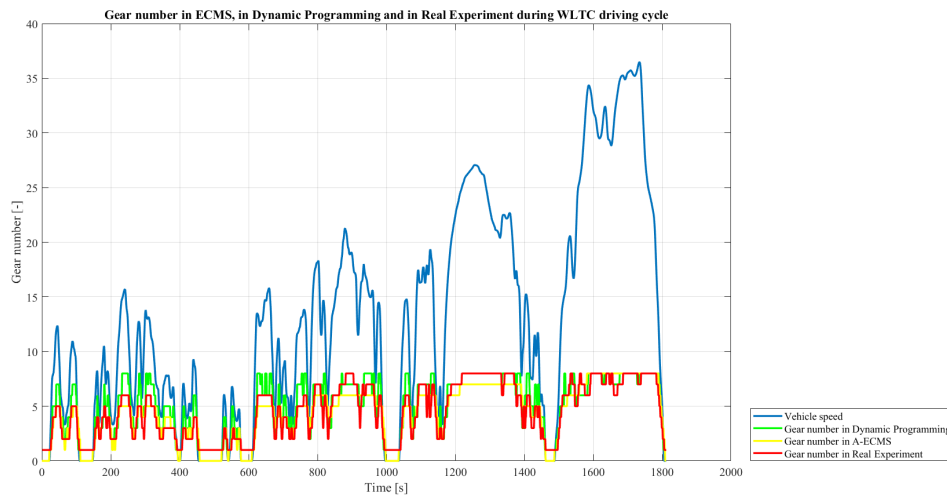


Figure 3.7: Gear number in ECMS, in DP and in Real Experiment, with Pure ICE mode during WLTC driving cycle

backward approach is not applicable, whereas that of the forward approach might be.

The backward modeling approach with the DP algorithm, in theory, provides an optimal trajectory of operational points for both ICE and the electric motor. However, its practical application is unfeasible. Nonetheless, the trajectory generated

Table 3.6: Model mismatch - RDE

Numerical results	FEV	CARS
Forward model mismatch on RDE	-1.993%	-7.474%
Backward model mismatch on RDE	-	-

by the DP algorithm serves as a crucial benchmark for evaluating the effectiveness of various EMS.

The forward modeling approach with ECMS optimizes the equivalent fuel consumption, which is a composite of the actual fuel consumption attributed to the ICE and the virtual fuel consumption resulting from the electric motor, at discrete time instants starting from the beginning of the driving cycle. ECMS with different s-factor controllers is the algorithm under comparison with the DP algorithm in this thesis. The effects of different s-factor controllers are the key points to compare, which directly influence the feasibility of using the ECMS algorithm in reality.

In addition to comparing different algorithms, several HEV architectures and electric motor configurations were also tested by using the backward approach, namely, DP to summarize a possible principle for designing the hardware.

3.6 Scope of Hybridization

This thesis includes a wide range of exploration of hybridization aspects in vehicles, including key components such as the electric motor, powertrain architecture, power-split algorithms between the ICE and electric motor, and the objective of hybridization, the details are as follows:

- **Electric Motor Specification:** The choice between 48V and 200V motors is an important decision regarding the voltage level of the motor. This choice has a significant impact on the performance and application of the motor. For example, batteries with higher voltage motors carry lower currents, extending battery life, while high voltage poses a higher safety risk to passengers inside the vehicle.
- **Powertrain Architecture Options:** In the field of hybrid vehicles, parallel hybrids feature the concurrent operation of both the ICE and electric motor, permitting cooperative or separate operation. On the contrary, series hybrids employ the electric motor to drive the vehicle, and the ICE is used to charge the battery and its function is independent from direct wheel propulsion. In addition, there are differences between the P1 and P2 classifications in the category of parallel architecture. In the P1 configuration, ICE and the motor share a common speed but may exhibit different torque outputs. In

contrast, the P2 architecture has a more intricate coupling between the ICE and the electric motor, facilitated by planetary gear systems and clutches which provides the choice between pure electric and ICE modes, as well as enabling battery charging through the ICE.

- **Energy Management Algorithm Considerations:** Among many energy management algorithms, the DP algorithm theoretically delivers an optimal trajectory of operational points for both the ICE and electric motor. But it is a backward approach that commences from the last discrete time instant to the first one of the driving cycle, necessitating substantial computational resources and thereby making practical applications infeasible. Nevertheless, the trajectory derived from the DP algorithm serves as a benchmark reference for assessing the performance of other EMS. Another part of the focus of this thesis centers on ECMS, characterized as a forward approach starting from the command of the driver. ECMS optimizes Equivalent Fuel Consumption at each discrete time instant from the beginning of the driving cycle. There are three different controllers in this research for ECMS to control the s-factor that is determinant for power split between ICE and electric motor: Relay-based switching logic, A-ECMS, and PID controller. ECMS serves as the algorithm compared with the DP algorithm in this thesis.
- **Primary Research Objective:** In this thesis, the most important focus is on reducing fuel consumption within the HEV system, and emission-related issues are beyond the specific scope of this study.

3.7 Choice of HEV architectures

Hybrid electric vehicles (HEV) have developed various architectures that combine ICE with electric propulsion systems. In this thesis, we delved into two main HEV architectures: P1 (Figure 3.1) and P2 (Figure 3.8), paired with two types of motors, 48V and 200V, respectively. By DP algorithm, we test the fuel consumption and battery state of charge (SOC) of hybrid electric vehicles with the following two architectures.

The characteristic of P1 48V architecture is the direct connection between ICE and electric motors. In this architecture, both the ICE and the 48V electric motor operate at the same speed but can provide different torque outputs. This architecture provides simplicity and reliability with lower potential safety hazards.

The P2 200V architecture adopts a complex coupling mechanism, using a planetary gear system and clutch to interconnect ICE and electric motors. This complex design allows for a choice between purely electric and pure ICE operating modes.

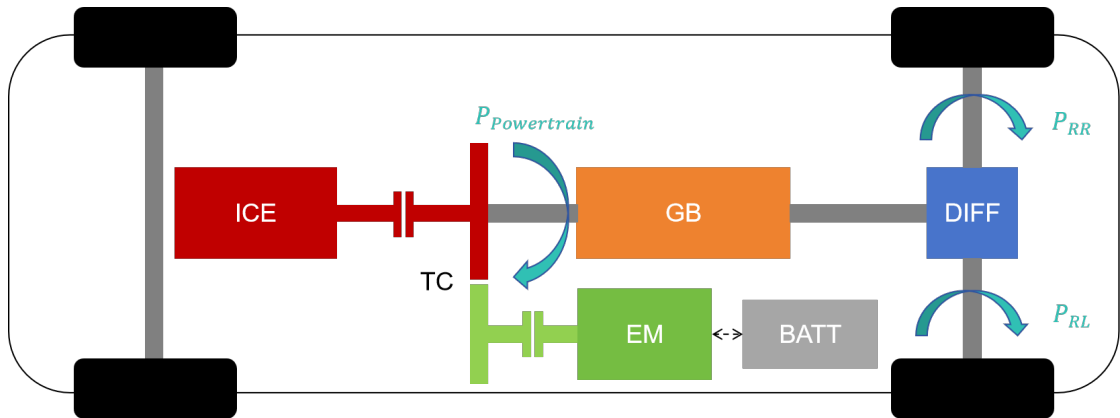


Figure 3.8: P2 architecture

3.8 Battery sizing

This article explores the impact of battery size on battery state of charge (SOC) and fuel consumption during the World Harmonized Light Vehicle Test Cycle (WLTC) in the configuration of the P1 48V architecture by using the DP algorithm. This test includes a range of battery sizes, ranging from 0.5 kWh to 3.0 kWh.

From a common sense perspective, larger batteries provide more benefits. However, it is evident that as the battery size approaches a certain threshold, the related advantages will weaken.

Chapter 4

Results & Discussion

This chapter concludes the performance test results of three controllers of the Equivalence Factor of the ECMS algorithm - relay-based switching logic, PID, and A-ECMS with P1 48V architecture, during the WLTC and the RDE driving cycle, including fuel consumption, battery state of charge (SOC), power flow, and energy contribution and loss. The performance of A-ECMS is emphasized to compare with the theoretical best performance obtained by the DP algorithm, providing a reference for optimizing the algorithm.

Apart from the P1 48V architecture, the performances of the P2 200V architecture and of the different battery sizes in the P1 48V architecture are also discussed in this chapter.

4.1 P1 48V architecture in the WLTC Cycle

The baseline of the Hybrid version of IVECO DAILY is P1 48V architecture. The test of the vehicle during the WLTC driving cycle is committed with 2 algorithms: DP and ECMS, respectively.

4.1.1 DP in WLTC driving cycle

In the vehicle model of DP, the state variables, which represent the vehicle system state, include the battery state of charge (SOC), and the previous gear number. The control variables, which are regarded as the control logic from one vehicle system state to another, are the gear number and the power-split factor. Minimizing fuel consumption while maintaining the battery state of charge (SOC) to a proper window to extend the battery life is the primary objective. Reducing frequent gear shifting that might wear the drive-train components by comparing the current gear number with the previous one using a penalty function is the secondary goal.

The fuel consumption of the vehicle using DP during the WLTC driving cycle is 2.263 L, and the SOC variation at the end of the driving cycle is 0 compared with the initial SOC value. Other detailed information is listed below. However, these results are merely the ideal conditions that are used as a reference to analyze other algorithms.

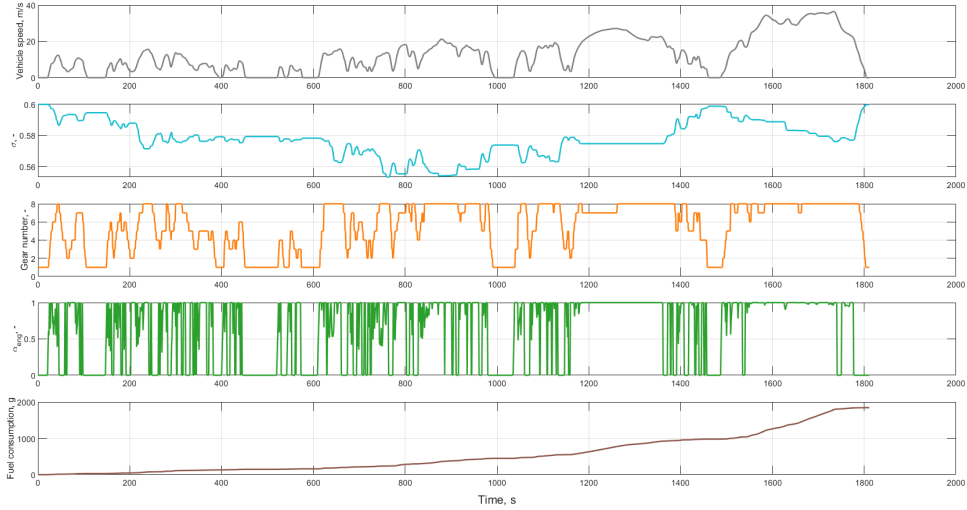


Figure 4.1: P1 48V Main profile with DP in WLTC

The first graph of Figure 4.1 illustrates the WLTC driving cycle, covering the urban, rural, and motorway driving conditions simultaneously. The vehicle speed fluctuates from 0 m/s to 40 m/s.

The second graph of Figure 4.1 shows the state of charge (SOC) of the battery with the initial value being 0.6. The state of charge ends up being 0.591 because of the state variable constraints defined in the DP control logic (from 0.59 to 0.61).

The third graph of Figure 4.1 depicts the gear number of the vehicle during the driving cycle. What is obvious is that the gear number strictly follows the vehicle speed over the driving cycle.

The fourth graph of Figure 4.1 represents the value of the power-split coefficient. As observed, the value of the power-split coefficient varies between 0 and 1 frequently when using the DP strategy. This means the engine starts and stops very frequently, which will result in energy loss and shorter component life.

The last graph of Figure 4.1 indicates the accumulation of fuel consumption during the drive cycle, which increases unsteadily due to some issues such as the varying vehicle speed, the intervention of the electric motor, etc.

The first graph of Figure 4.2 shows different power modes at different speeds. It can be observed that the "pure electric" mode is typically used for braking conditions.

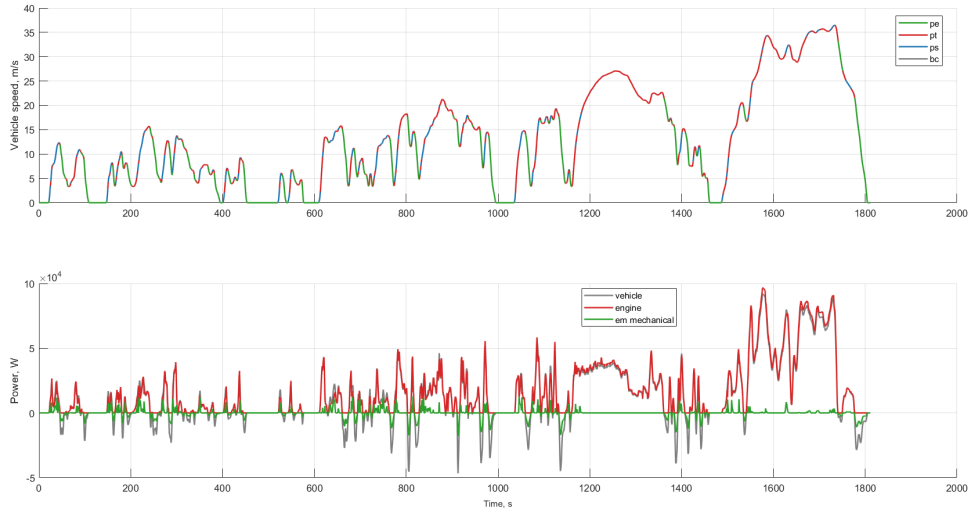


Figure 4.2: P1 48V Power profile with DP in WLTC

Whereas the "power-split" mode is mostly used for acceleration, especially at high speeds when the engine and electric motor work together. The "pure thermal" mode is applied when the vehicle speed is high or the vehicle is accelerating. And, the battery charges when braking in "pure electric" mode. This can be seen by looking at the SOC graph in the main profile and the power graph below.

The second graph of Figure 4.2 shows the variation of power of the vehicle, engine, and electric motor during the drive cycle. If the power of the vehicle is negative, it indicates that the vehicle is decelerating. If the power of the electric motor is negative, the motor acts as a generator and the battery is charged. However, the thermal engine cannot have negative power.

4.1.2 DP vs. ECMS in WLTC driving cycle

Table 4.1 lists the fuel consumption of the 4 different algorithms and their final SOC variation at the end of the driving cycle. A-ECMS exhibits the least deviation in fuel consumption from DP, primarily because of its sufficient use of the electric motor during the low-speed region of the WLTC driving cycle as evidenced by the SOC trend shown in the following figure. The final SOC of A-ECMS is approximately 60.5%, while the SOC of the relay-based switching logic is 59.8%. In contrast, PID ultimately recorded a 5% SOC change, which is the highest SOC limit. Further detailed comparisons of various parameters are provided below.

Table 4.1: P1 48V architecture performance - WLTC

Performance - WLTC	DynaProg	A-ECMS	Relay	PID
Fuel consumption [L]	2.263	2.329	2.335	2.345
Fuel consumption gap	Reference	+2.916%	+3.182%	+3.624%
SOC variation [%]	0	+0.654%	-0.153%	+5.000%

Comparison of engine operating points with DP and A-ECMS

Figure 4.3 illustrates the engine map, showing a significant difference in control logic between DP and A-ECMS. The x-axis and y-axis represent engine speed and engine torque, respectively. For each engine speed, the corresponding maximum engine torque is limited due to engine performance. The contour curves in Figure 4.3 represent different normalized Brake Specific Fuel Consumption (BSFC) at each engine speed and torque, with lower normalized BSFC indicating lower fuel consumption at the same engine power. The OOL of the engine is shown by the dashed curve in Figure.

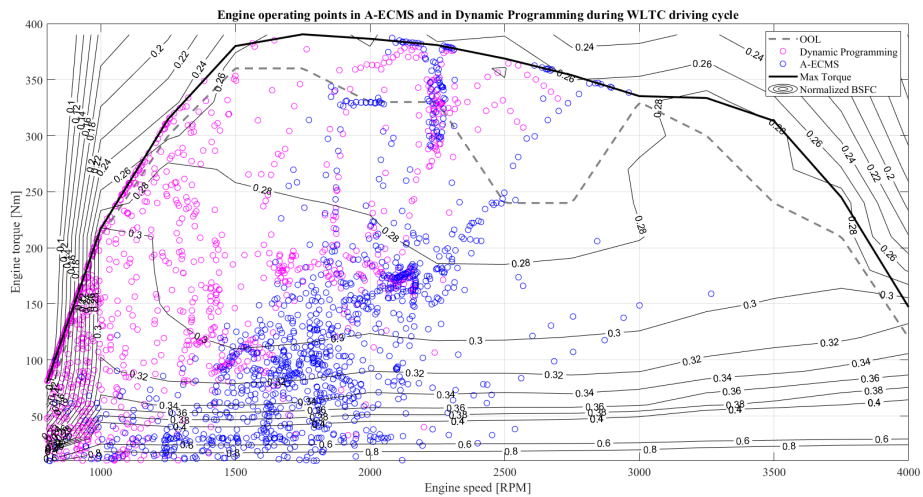


Figure 4.3: P1 48V Engine operating points of DP and A-ECMS during WLTC driving cycle

The purple points in the map refer to the engine operating points using DP. It can be observed that the engine is working at a relatively lower speed and higher torque and the operating points are rather close to the OOL compared with A-ECMS, where the most of normalized BSFC of operating points in DP is lower than 0.32, while a considerable portion of operating points in A-ECMS (blue

points) are located at the area where the normalized BSFC is higher than 0.32.

The reason why the distributions of operating points in DP and A-ECMS are different can be inferred from the following comparison of engine power flows, engine torque, and gear shifting logic. In brief, DP renders higher gear numbers over the driving cycle, which results in lower engine speed and higher engine torque, bringing the operating points closer to OOL and, thereby, reducing fuel consumption.

Comparison of power flows and torque of ICE with DP and A-ECMS

Figure 4.4 and Figure 4.5 compare the engine power profile and engine torque profile between DP and A-ECMS at each time instant over the driving cycle, respectively.

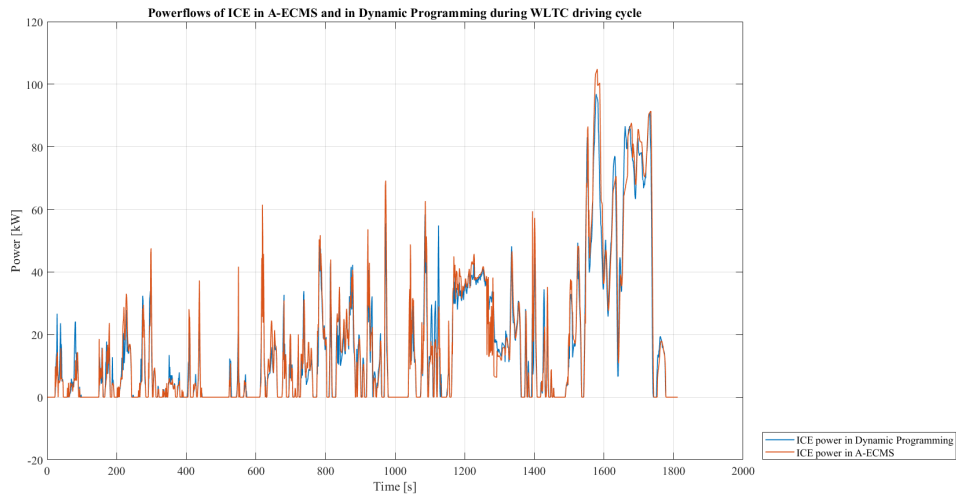


Figure 4.4: P1 48V Power flows of ICE in A-ECMS and DP during WLTC driving cycle

In comparison to A-ECMS, DP (blue curve) results in the engine operating at higher torque with basically the same power. This leads to a lower engine speed, as indicated by the relationship between engine power, engine speed, and engine torque. The characteristic of lower engine speed observed in DP aligns with the trends identified in the comparison of engine operating points.

Comparison of gear shifting with DP and A-ECMS

Figure 4.6 shows the gear-shifting logic of DP and A-ECMS over the WLTC driving cycle.

When comparing DP with its corresponding A-ECMS, an intriguing discovery emerged. As demonstrated by Figure 4.6, DP (green curve) consistently favors

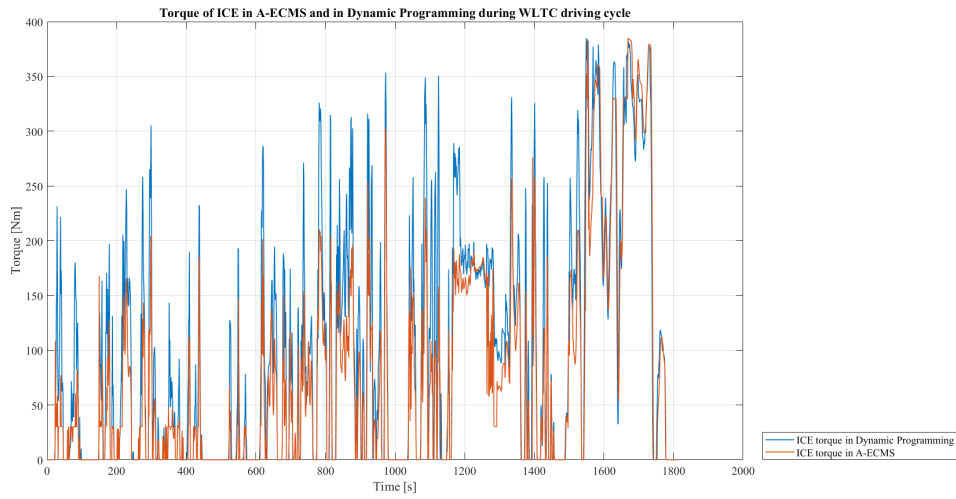


Figure 4.5: P1 48V Torque of ICE in A-ECMS and DP during WLTC driving cycle

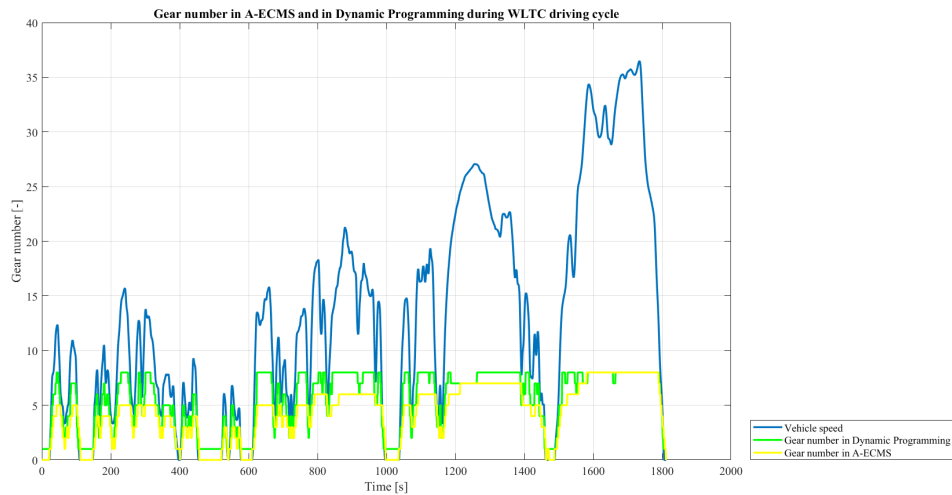


Figure 4.6: P1 48V Gear numbers in A-ECMS and DP during WLTC driving cycle

higher gears over the entire driving cycle. This preference for higher gear numbers translates into a unique operating mode where the engine maintains a lower speed and higher torque level during vehicle propulsion. This tendency is rooted in the pursuit of optimizing fuel efficiency. The principle is straightforward: by selecting a higher gear number, DP reduces engine speed and increases engine torque, ensuring

the engine operates closer to OOL, which makes DP significantly different from A-ECMS in the field of shift logic.

Comparison of power flows and torque of electric motor with DP and A-ECMS

Figure 4.7 and Figure 4.8 compare the electric motor power profile and electric motor torque profile between DP and A-ECMS at each time instant over the driving cycle, respectively.

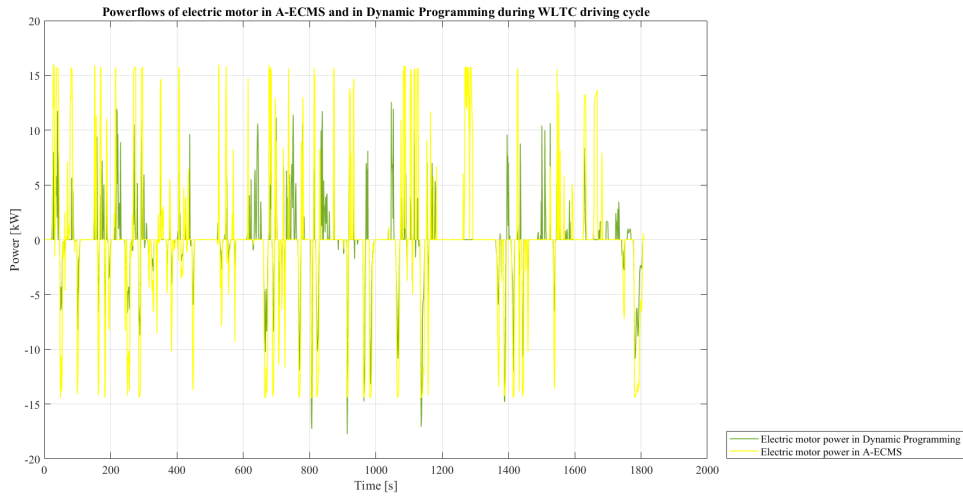


Figure 4.7: P1 48V Power flows of electric motor in A-ECMS and DP during WLTC driving cycle

A notable difference emerges in the behavior of the electric motor. The illustration demonstrates that DP (green curve) consistently opts for lower electric power while simultaneously achieving higher levels of torque. Moreover, DP adopts a less aggressive approach that is more favorable for battery health.

Comparison of fuel consumption with DP and ECMS

Figure 4.9 provides an overview of fuel consumption accumulation under various energy management algorithms throughout the driving cycle. The green curve represents the theoretically optimal fuel consumption achieved through DP. Additionally, the performances of three equivalence factor controllers: A-ECMS, PID controller, and Relay-based switching logic, are compared to DP, depicted by three distinct curves in Figure, each distinguished by its color.

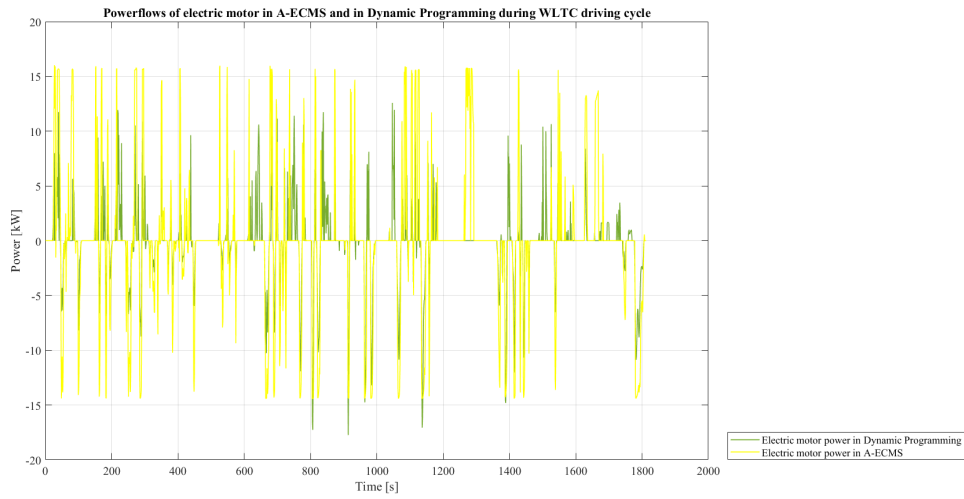


Figure 4.8: P1 48V Torque of electric motor in A-ECMS and DP during WLTC driving cycle

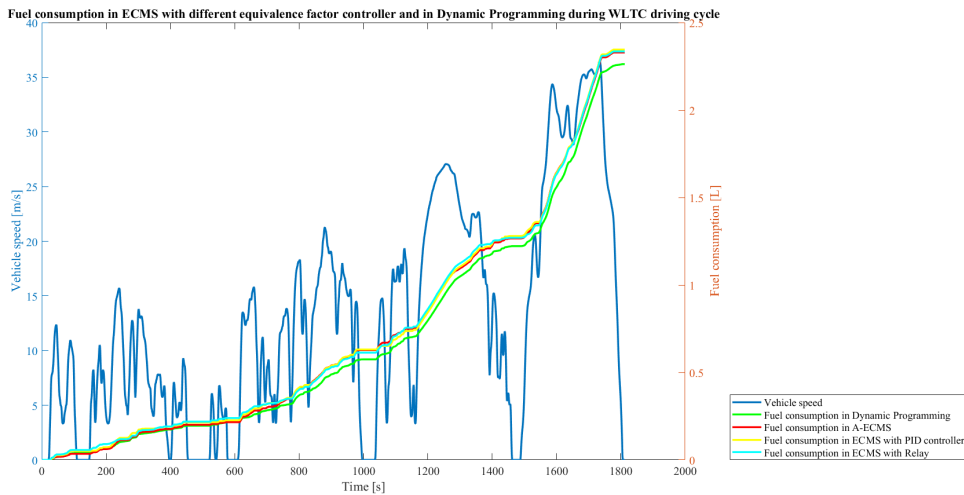


Figure 4.9: P1 48V Fuel consumption in A-ECMS and DP during WLTC driving cycle

The A-ECMS controller exhibits the most efficient fuel consumption, particularly in the low-speed region of the driving cycle, where it closely approaches the efficiency of DP. Conversely, the PID controller yields the highest fuel consumption. Towards the conclusion of the driving cycle, the fuel consumption performances of the three controllers are close.

Comparison of SOC with DP and ECMS

The battery SOC, an essential parameter in this context, reflects the energy level of the battery throughout a driving cycle. Figure 4.10 demonstrates the SOC trends during the WLTC driving cycle for four different energy management algorithms.

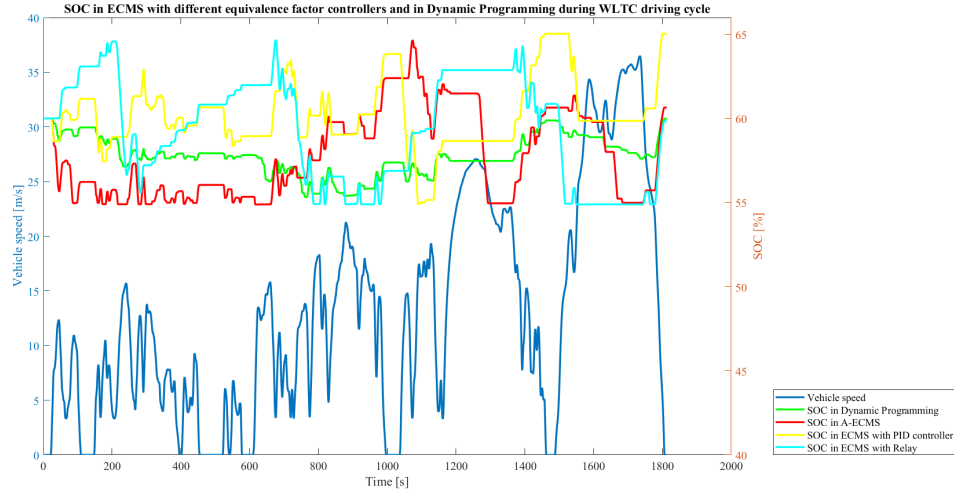


Figure 4.10: P1 48V SOC variation in A-ECMS and DP during WLTC driving cycle

The characteristics of the 4 algorithms in terms of SOC are the following:

- DP: DP adopts a stable SOC variation approach throughout the driving cycle. It avoids aggressive SOC fluctuations, ensuring a consistent SOC level from the beginning to the end of the cycle.
- Adaptive ECMS: The A-ECMS exhibits a strong tendency for battery usage during low-speed driving phases, which resembles the DP, and charges the battery during medium and high-speed regions. Despite these variations, A-ECMS maintains SOC stability, with no significant SOC variation observed at the end of the driving cycle.
- The ECMS with Relay-based switching logic: The ECMS with Relay-based switching logic initially operates without using the electric motor. Subsequently, it follows an aggressive approach with sharp electric motor usage. Remarkably, despite this aggressiveness, no significant SOC variation is observed at the end of the driving cycle.
- ECMS with PID controller: The ECMS with PID controller pursues to maintain the target SOC, but exhibits greater SOC changes after the driving

cycle at the end of the cycle, due to strong braking, the SOC increases sharply to approximately 65%. Compared with other algorithms, this s-factor controller has a relatively large change in SOC.

Overall, DP prioritizes SOC stability and battery health, A-ECMS tends to explore the battery potential at low vehicle speed, ECMS with Relay-based switching logic takes less usage of the electric motor at the beginning of the driving cycle, and ECMS with PID Controller shows more significant SOC variations due to its PID control strategy.

Comparison of energy contribution and loss with DP and A-ECMS

Figure 4.11 and Figure 4.12 illustrate the energy sources powering the powertrain in the DP and A-ECMS algorithm during the WLTC driving cycle, respectively. In the A-ECMS algorithm, the majority of the energy to the powertrain is delivered by an Internal Combustion Engine (ICE), about 92%. The electric motor provides 7% of the total energy for propulsion of the vehicle, while nearly 1% of the total powertrain energy is lost due to the electric motor. While the energy provided by the ICE takes up more proportion in the DP algorithm (95%). Table 4.2 shows the energy contribution in the 4 conditions with different algorithms and s-factor controllers.

Table 4.2: P1 48V architecture Energy contribution in WLTC driving cycle

Energy Contributions - WLTC [kWh]	DynaProg	A-ECMS	Relay	PID
Energy delivered by ICE	7.994	8.312	8.311	8.405
Energy delivered by electric motor	0.335	0.639	0.649	0.566
Energy delivered by powertrain	8.328	8.951	8.961	8.971
Electric motor loss	0.050*	0.099	0.096	0.092
Regenerative energy	-0.414	-0.828	-0.828	-0.812

*The Electric motor loss is Electric motor loss + battery loss for all DP cases.

In terms of energy losses in A-ECMS (Figure 4.13 and Figure 4.14, aerodynamic drag, primarily occurring during the high-speed phase at the end of the cycle, contributes to over 50% of the total loss. Driveline losses and rolling resistance evenly split the remaining half, accounting for 17% and 24%, respectively, while electric motor losses are less than 1%. The loss due to the drive-train in DP is only 6%, which might be due to the different modeling processes in the drive-train. Table 4.3 shows the energy loss in the 4 conditions with different algorithms and s-factor controllers.

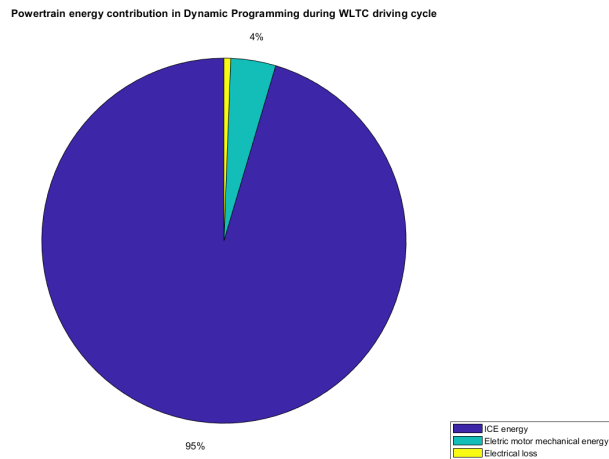


Figure 4.11: P1 48V Energy contribution in DP during WLTC driving cycle

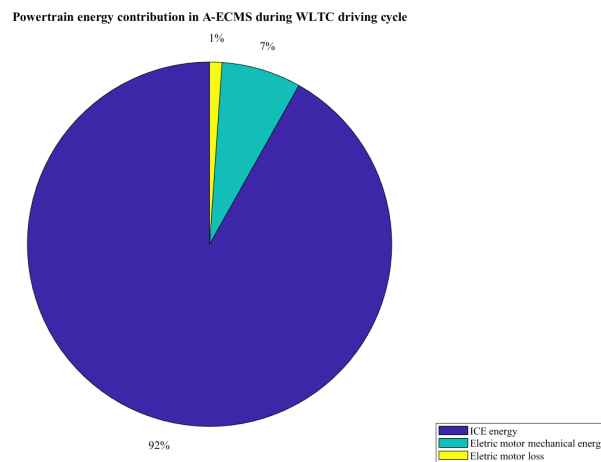


Figure 4.12: P1 48V Energy contribution in A-ECMS during WLTC driving cycle

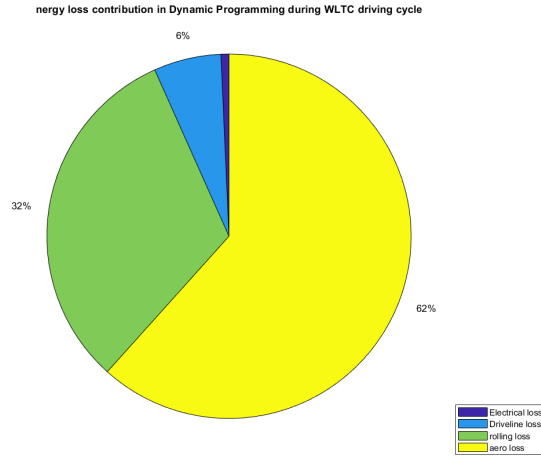
Comparison of available regenerative energy in DP and A-ECMS

Figure 4.15 and Figure 4.16 show the theoretically available energy that can be used for regeneration in DP and A-ECMS, respectively.

The potential of using regenerative braking for energy recovery is equal to the amount of kinetic and potential energy that needs to be dissipated, minus the amount dissipated due to rolling and aerodynamic resistance.

Table 4.3: P1 48V architecture Energy loss in WLTC driving cycle

Energy Losses - WLTC [kWh]	DynaProg	A-ECMS	Relay	PID
Aerodynamic loss	4.344	4.302	4.300	4.296
Rolling loss	2.231	1.776	1.776	1.775
Electric motor loss	0.050	0.099	0.096	0.092
Driveline loss	0.421	1.275	1.249	1.259

**Figure 4.13:** P1 48V Energy loss in DP during WLTC driving cycle

After subtracting the aerodynamic loss and rolling loss, the remaining part of the powertrain energy can be regarded as potentially available energy for regeneration[24], which is about 32% of the total energy in A-ECMS. On the other side, due to the higher rolling loss in the DP model, a lower theoretically available energy for regenerative braking is observed, nearly half of that in A-ECMS.

Summary of P1 48V architecture with DP and ECMS in WLTC Cycle

This section of the thesis evaluates the performance of three Equivalence Factor controllers, namely Relay-based switching logic, PID, and A-ECMS, in the context of the ECMS algorithm throughout the WLTC driving cycle. A primary focus is placed on A-ECMS, which is closely compared to the theoretically optimal DP algorithm.

The assessment encompasses key parameters, including fuel consumption, battery state of charge (SOC), power flow, energy contributions, and losses. The analysis reveals that DP consistently favors lower engine speed and higher torque, closing

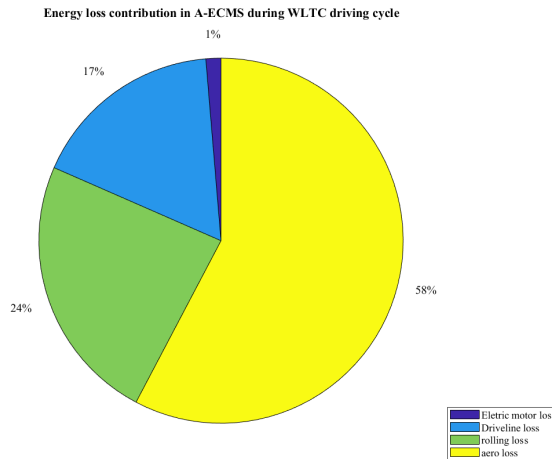


Figure 4.14: P1 48V Energy loss in A-ECMS during WLTC driving cycle

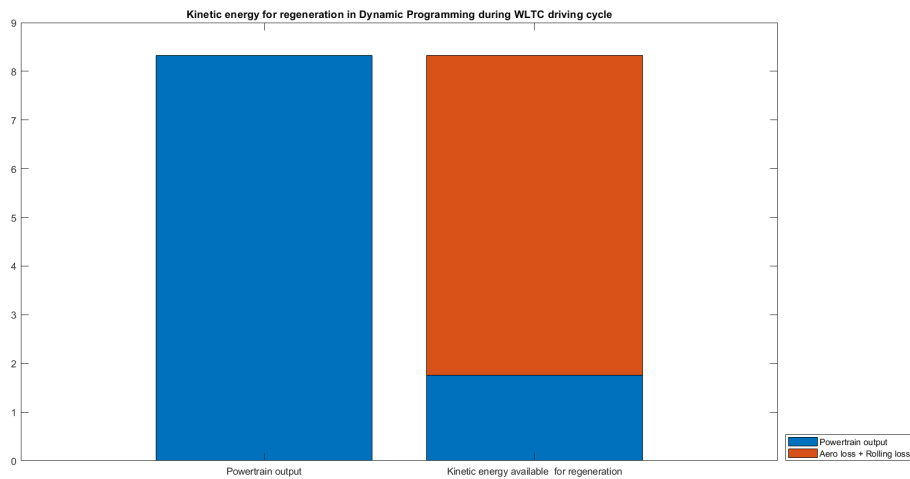


Figure 4.15: P1 48V Kinetic energy in DP during WLTC driving cycle

to the OOL, and reducing fuel consumption, while A-ECMS explores the battery’s potential during low-speed phases. Moreover, the less aggressive approach adopted by DP is more battery-friendly. The SOC profiles illustrate the stability of DP compared to A-ECMS, showing its prioritization of battery health.

In addition, the high-speed region of the WLTC cycle results in high aerodynamic loss which accounts for over half of the total. One-third of the powertrain energy can be theoretically recycled for regeneration in the case of A-ECMS.

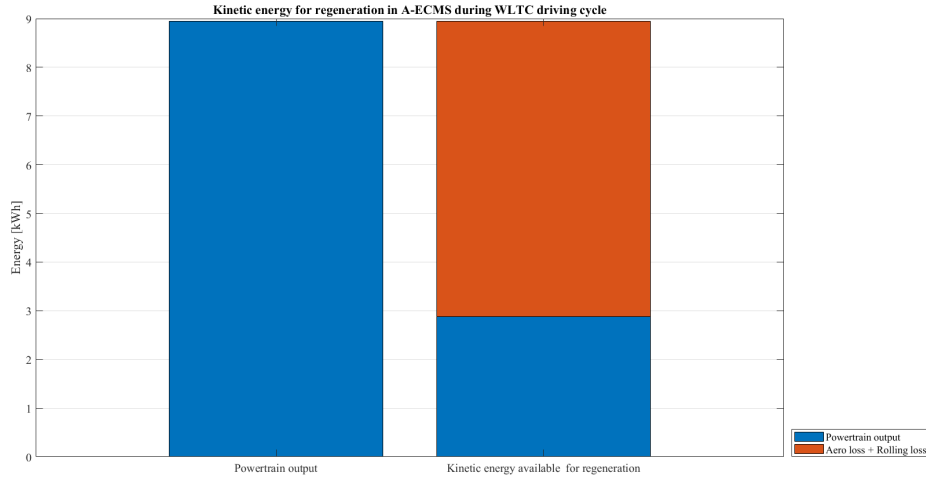


Figure 4.16: P1 48V Kinetic energy in A-ECMS during WLTC driving cycle

Overall, the A-ECMS controller has shown good prospects in using batteries at low speeds, but there is still a significant gap compared to the theoretical optimal control strategy, DP.

4.2 P1 48V architecture in the RDE Urban Cycle

RDE Urban cycle is characterized by low speed and frequent accelerations. As shown in Figure 4.17, the operating points of DP (purple), which are closer to OOL, are far better than those of A-ECMS (blue) in terms of BSFC. A-ECMS has the smallest fuel consumption gap with DP among the 3 s-factor controllers, shown in Table 4.4

Table 4.4: P1 48V architecture performance - RDE Urban

Performance - RDE Urban	DynaProg	A-ECMS	Relay	PID
Fuel consumption [L]	0.657	0.703	0.712	0.705
Fuel consumption gap	Reference	+7.001%	+8.371%	+7.306%
SOC variation [%]	-0.648%	-0.022%	+2.658	+0.606%

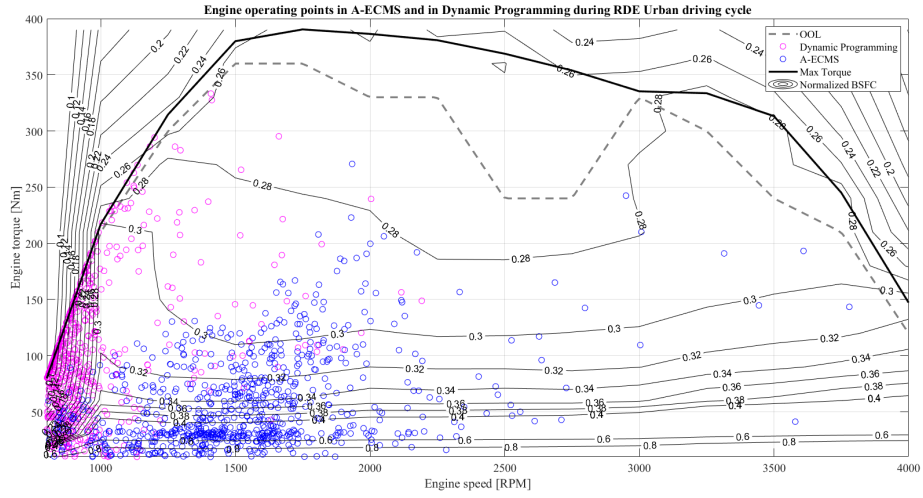


Figure 4.17: P1 48V Engine operating points of DP and A-ECMS during RDE Urban driving cycle

4.2.1 Comparison of power flows of ICE with DP and A-ECMS

The power flow of ICE in DP during the RDE Urban driving cycle basically resembles that in A-ECMS, as plotted in Figure 4.18. The slightly different power flows of them are due to the different usage of the electric motor.

4.2.2 Comparison of power flows of the electric motor with DP and A-ECMS

The phenomenon is similar to the result in the WLTC driving cycle, DP has lower power but higher torque, as Figure 4.19 shows. The DP still exhibits a more stable utilization of the electric motor and, therefore a more stable utilization of the battery as well.

4.2.3 Comparison of SOC with DP and A-ECMS

Figure 4.20 demonstrates the SOC fluctuation when using DP and ECMS with 3 different s-factor controllers. A-ECMS uses the motor at the beginning of the driving cycle and then charges the battery when it is depleted to the lower limit of the SOC window. While the PID controller maintains the SOC around 60% with no significant fluctuation. Additionally, the Relay-based switching logic charges the battery at the beginning of the driving cycle and has a sharp decrease and increase

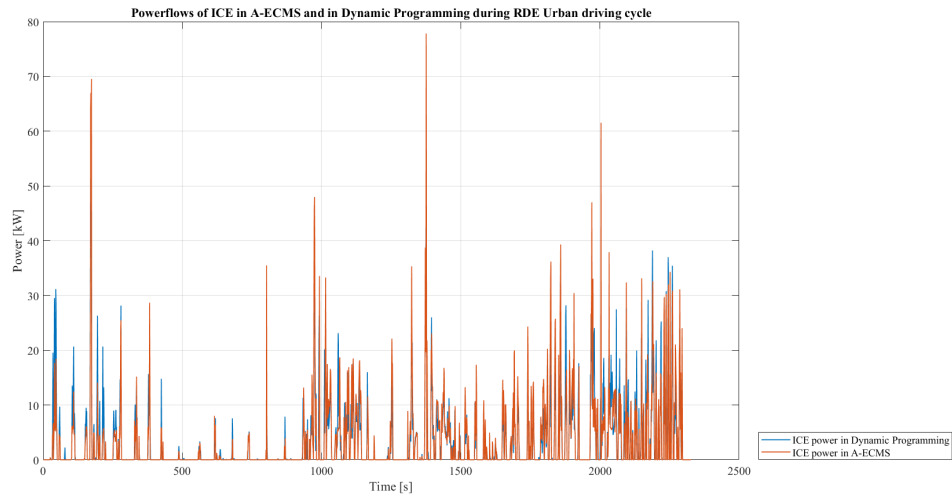


Figure 4.18: P1 48V Power flows of ICE in DP and A-ECMS during RDE Urban driving cycle

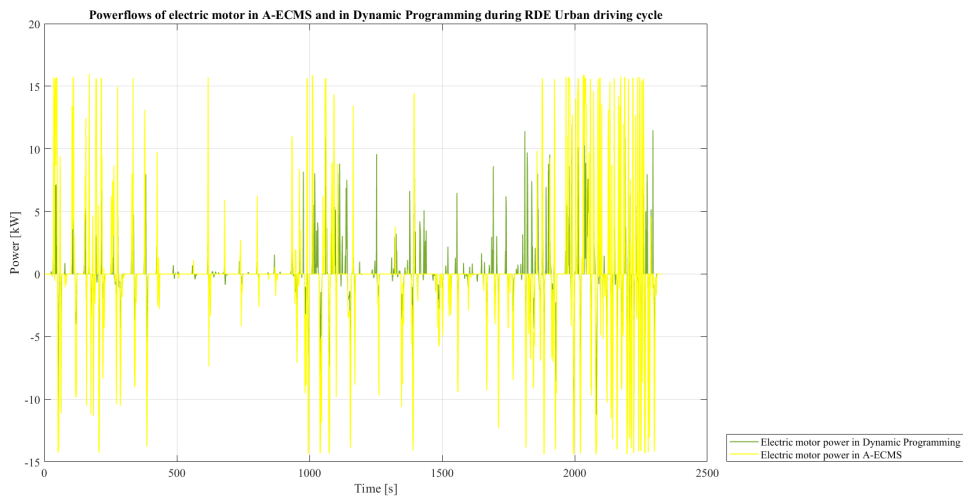


Figure 4.19: P1 48V Power flows of the electric motor in DP and A-ECMS during RDE Urban driving cycle

of SOC, finally, the SOC ends with 62.7%. Lastly, DP is as stable as it works in WLTC.

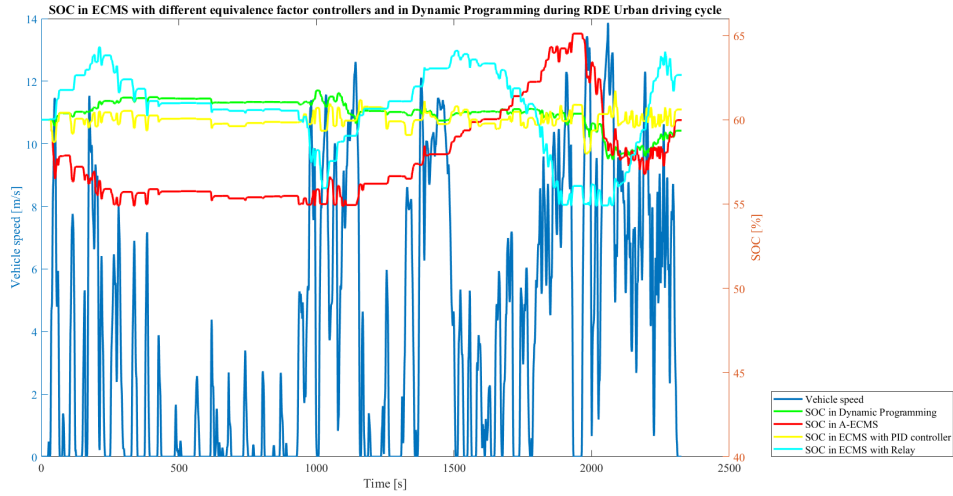


Figure 4.20: P1 48V SOC in DP and A-ECMS during RDE Urban driving cycle

4.2.4 Comparison of fuel consumption with DP and A-ECMS

The fuel consumption of A-ECMS is even lower than that of DP at the beginning of the driving cycle, but due to a finite SOC window, the battery needs to be charged afterward, resulting in higher fuel consumption during battery charging. Finally, A-ECMS has the smallest gap with DP in terms of fuel consumption, which is illustrated and compared to other s-factor controllers in Figure 4.21.

4.2.5 Energy contribution and loss with A-ECMS

The energy delivered by the electric motor during the RDE Urban driving cycle accounts for 20% of the total, which is higher than that in the WLTC driving cycle, shown in Figure 4.22. The detailed comparison is listed in Table 4.5.

Table 4.5: P1 48V architecture Energy contribution in RDE Urban driving cycle

Energy - RDE Urban [kWh]	DynaProg	A-ECMS	Relay	PID
Energy delivered by ICE	2.099	2.141	2.176	2.179
Energy delivered by electric motor	0.284	0.585	0.545	0.572
Energy delivered by powertrain	2.383	2.726	2.721	2.751
Regenerative energy	-0.346	-0.725	-0.720	-0.748

As for the perspective of energy loss (Figure 4.23), the rolling loss takes the

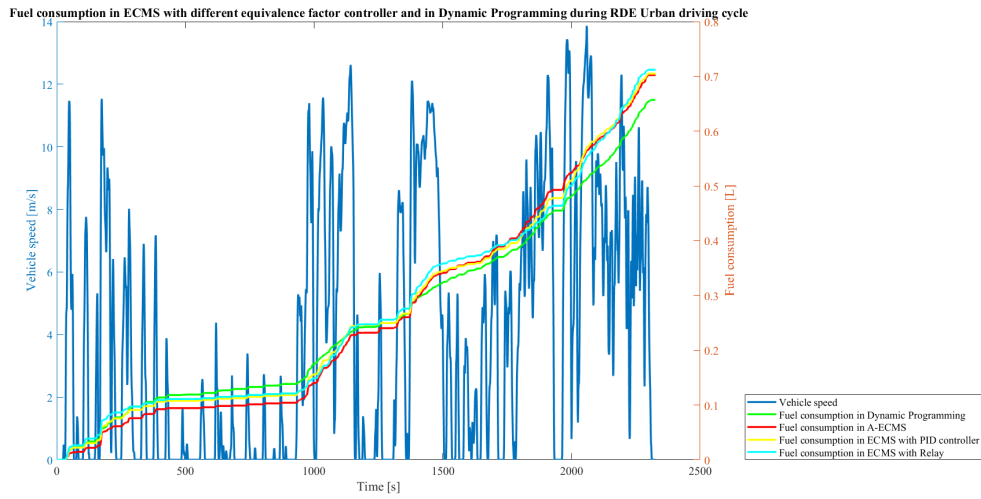


Figure 4.21: P1 48V Fuel consumption in DP and A-ECMS during RDE Urban driving cycle

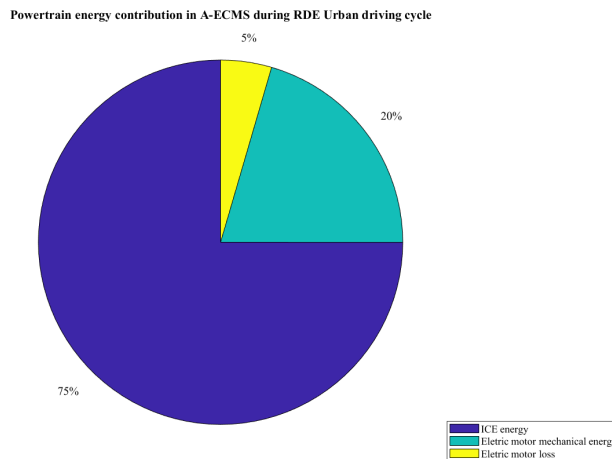
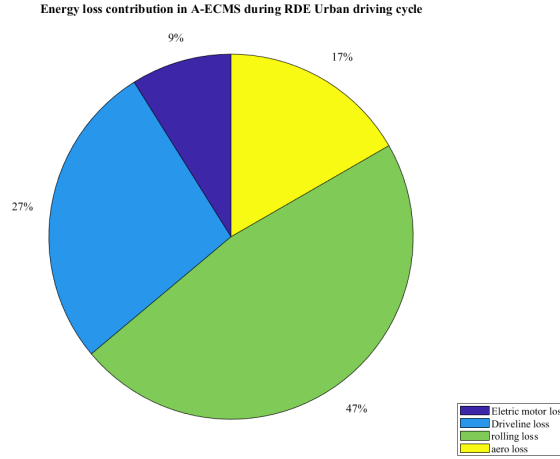


Figure 4.22: P1 48V Energy contribution in A-ECMS during RDE Urban driving cycle

dominance of the loss contribution, with 47%. The aerodynamic loss only takes up 17% of the total loss, which is because of the low-speed feature of the RDE Urban driving cycle. The comparison of energy loss during the RDE Urban driving cycle with different conditions is in Table 4.6.

Table 4.6: P1 48V architecture Energy loss in RDE Urban driving cycle

Energy Losses RDE Urban [kWh]	DynaProg	A-ECMS	Relay	PID
Aerodynamic loss	0.241	0.241	0.241	0.241
Rolling loss	0.855	0.683	0.683	0.683
Electric loss	0.038	0.100	0.129	0.104
Driveline loss	0.128	0.393	0.385	0.424

**Figure 4.23:** P1 48V Energy loss in A-ECMS during RDE Urban driving cycle

4.2.6 Available regenerative energy in A-ECMS algorithm

Figure 4.24 shows that more than half of the kinetic energy can be recycled for regeneration from a theoretical point of view in the RDE Urban driving cycle, due to the low aerodynamic loss. This means the energy regeneration potential is very high in urban conditions.

4.2.7 Summary of P1 48V architecture with DP and ECMS in the RDE Urban Cycle

The A-ECMS controller sufficiently utilizes the electric motor and battery, then recharges the battery when SOC is approaching the lower limit in the RDE Urban driving cycle. The PID controller is still strong enough to keep the SOC around the target level. And the Relay-based switching logic still recharges the battery at the beginning. The performance of fuel consumption and SOC variation in this driving cycle when using the A-ECMS controller is the best of the three.

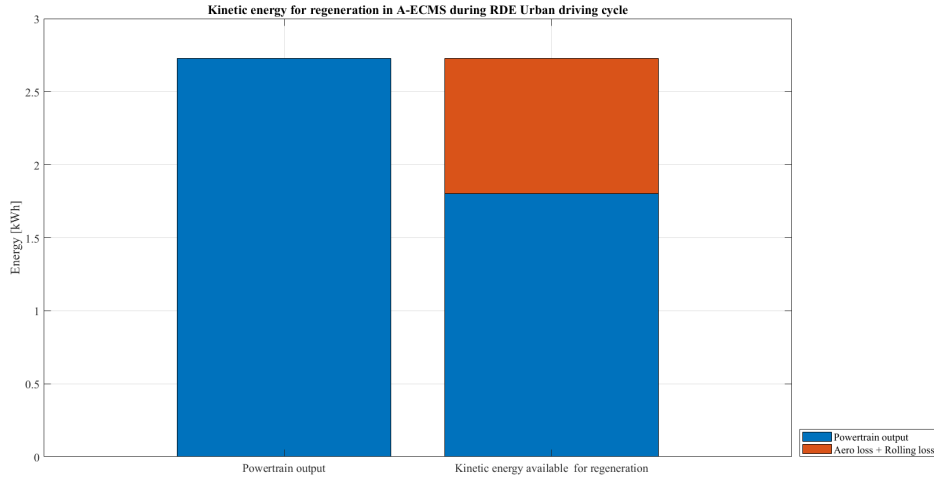


Figure 4.24: P1 48V Kinetic energy in A-ECMS during RDE Urban driving cycle

To put it simply, the A-ECMS controller is prone to use the electric motor during the RDE Urban driving cycle. The PID controller is still aggressive and strong.

4.3 P1 48V architecture in the RDE Rural Cycle

RDE Rural cycle is composed of medium-to-high speed profiles, examining the vehicle in rural conditions, but it is down-scaled due to the constraints of vehicle performance. In the RDE Rural cycle, the operating points with DP are still better than those in A-ECMS, which is, anyway, not as dramatic as it is in the RDE Urban cycle, as illustrated in Figure 4.25.

Table 4.7 lists the performance of DP and ECMS with different s-factor controllers. The PID controller enables the lowest fuel consumption gap with DP. However, the difference between these 3 controllers is not obvious.

Table 4.7: P1 48V architecture performance - RDE Rural

Performance - RDE Rural	DynaProg	A-ECMS	Relay	PID
Fuel consumption [L]	1.910	2.016	2.012	2.009
Fuel consumption gap	Reference	+5.550%	+5.340%	+5.183%
SOC variation [%]	-0.340%	+1.628%	+1.429%	+0.952%

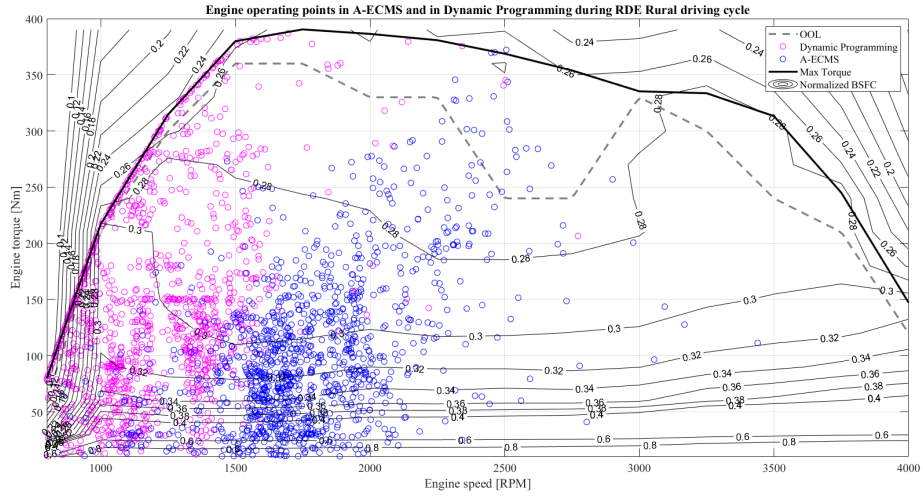


Figure 4.25: P1 48V Engine operating points of DP and A-ECMS during RDE Rural driving cycle

4.3.1 Comparison of power flows of ICE with DP and A-ECMS

As for the power flow of ICE during the RDE Rural driving cycle (Figure 4.26), the power flows of ICE when using DP and A-ECMS are almost the same, but DP still has a higher torque profile.

4.3.2 Comparison of power flows of the electric motor with DP and A-ECMS

Similar to the previous driving cycles, DP renders lower electric motor power but higher electric motor torque in the RDE Rural driving cycle, as plotted in Figure 4.27.

4.3.3 Comparison of SOC with DP and A-ECMS

When it comes to the SOC variation during the RDE Rural driving cycle (Figure 4.28), what is consistent with previous driving cycles is that the A-ECMS uses a motor at the beginning of the driving cycle and then charges it when the battery runs out. The PID controller charges the battery during the braking process and then maintains SOC without significant fluctuations. The SOC change of the relay-based switching logic still shows a sharp decrease and increase, ultimately ending at 61.4%. Besides, DP is as stable as previous driving cycles.

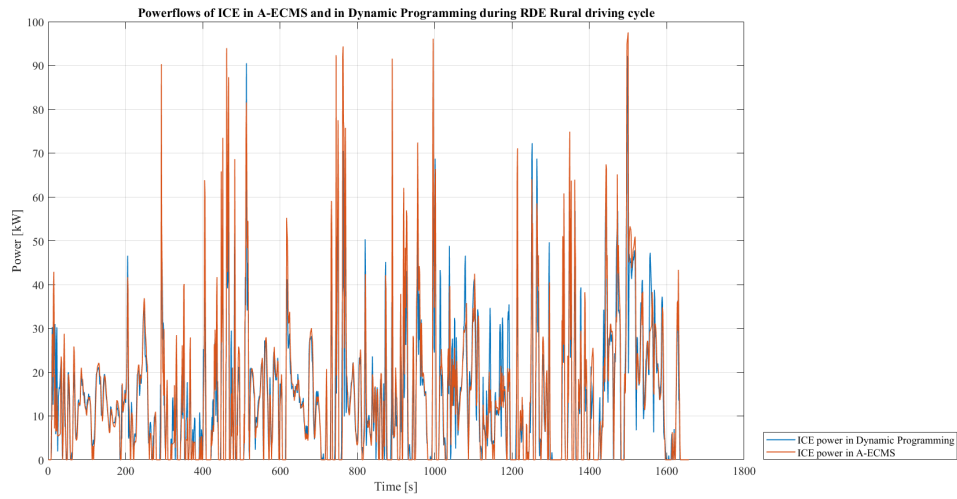


Figure 4.26: P1 48V Power flows of ICE in DP and A-ECMS during RDE Rural driving cycle

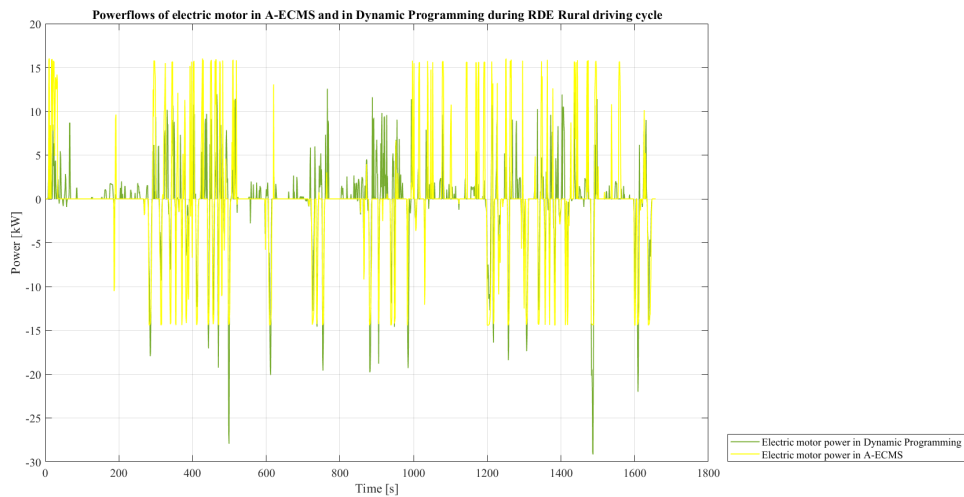


Figure 4.27: P1 48V Power flows of the electric motor in DP and A-ECMS during RDE Rural driving cycle

4.3.4 Comparison of fuel consumption with DP and A-ECMS

A-ECMS is prone to utilize the battery and recharge it, resulting in higher fuel consumption at the rear part of the cycle. Overall, the 3 controllers have similar

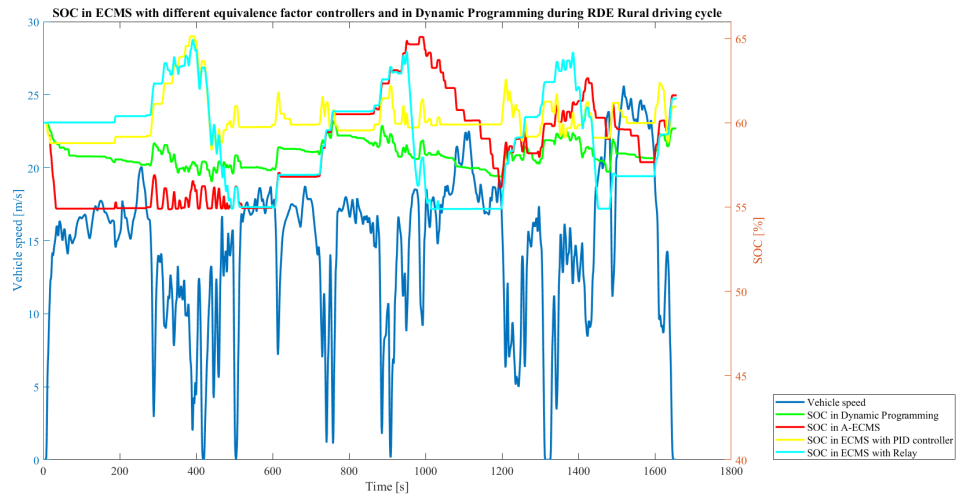


Figure 4.28: P1 48V SOC in DP and A-ECMS during RDE Rural driving cycle

fuel consumption in the RDE Rural driving cycle, which can be seen from Figure 4.29. This is due to the fewer opportunities for the electric motor to power the vehicle compared to the RDE Urban driving cycle.

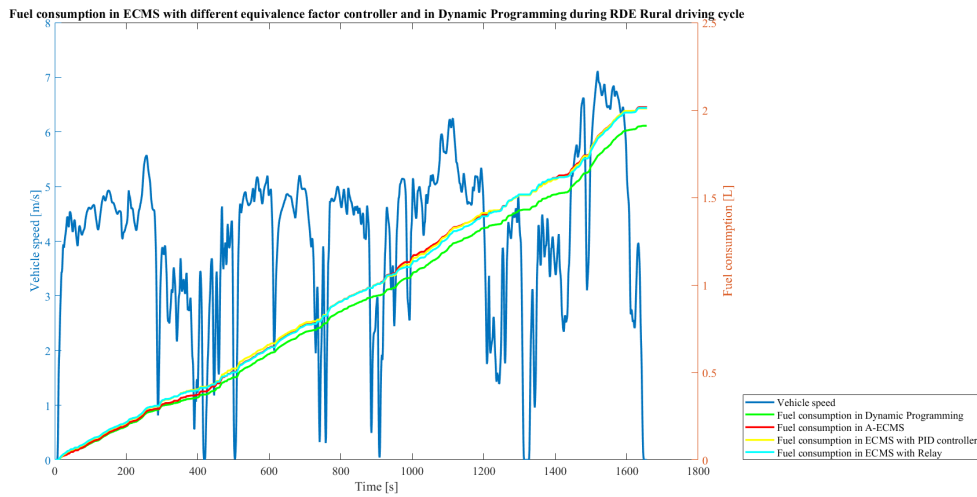


Figure 4.29: P1 48V Fuel consumption in DP and A-ECMS during RDE Rural driving cycle

4.3.5 Energy contribution and loss with A-ECMS

The electric motor provides 7% of the total energy for propulsion (see Figure 4.30), and the majority of energy is still delivered by ICE. Table 4.8 lists the energy contribution of each component of the powertrain with different algorithms and s-factor controllers. Moreover, Figure 4.31 presents the energy loss distribution, where the aerodynamic loss and rolling loss are both significant during the RDE Rural cycle, with 44% and 32% respectively. The detailed losses are presented in Table 4.9.

Table 4.8: P1 48V architecture Energy contribution in RDE Rural driving cycle

Energy - RDE Rural [kWh]	DynaProg	A-ECMS	Relay	PID
Energy delivered by ICE	6.543	6.927	6.898	6.905
Energy delivered by electric motor	0.424	0.569	0.585	0.576
Energy delivered by powertrain	6.966	7.496	7.483	7.481
Regenerative energy	-0.570	-0.765	-0.783	-0.764

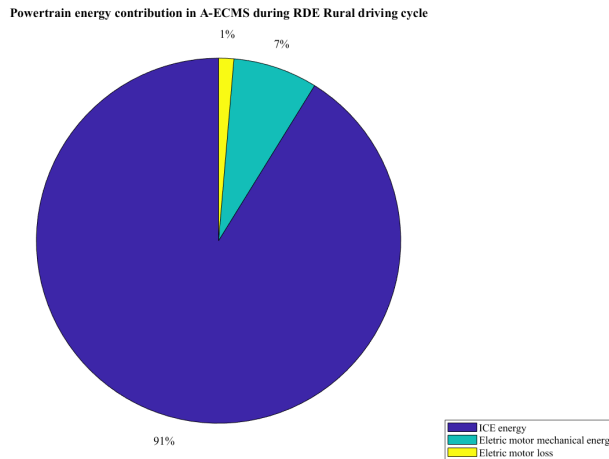


Figure 4.30: P1 48V Energy contribution in A-ECMS during RDE Rural driving cycle

4.3.6 Available regenerative energy in A-ECMS algorithm

Near half of the kinetic energy can be recycled in the RDE Rural cycle, which is less than that in the RDE Urban cycle and similar to the WLTC cycle, as shown

Table 4.9: P1 48V architecture Energy loss in RDE Rural driving cycle

Energy Losses RDE Rural [kWh]	DynaProg	A-ECMS	Relay	PID
Aerodynamic loss	2.520	2.514	2.514	2.514
Rolling loss	2.304	1.836	1.836	1.836
Electric loss	0.038	0.102	0.102	0.100
Driveline loss	0.353	1.259	1.263	1.248

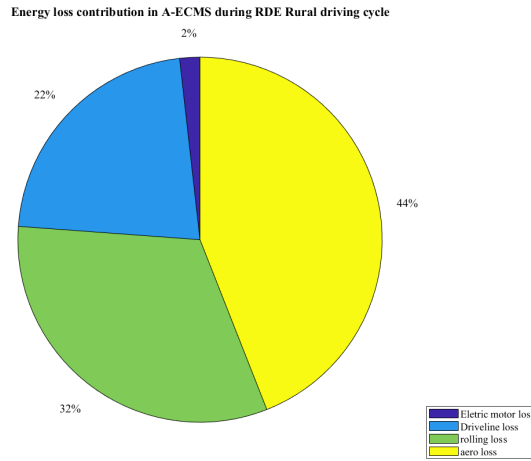


Figure 4.31: P1 48V Energy loss in A-ECMS during RDE Rural driving cycle

in Figure 4.32. It is due to the high aerodynamic losses caused by the medium and high-speed section of the RDE rural cycle.

4.3.7 Summary of P1 48V architecture with DP and ECMS in the RDE Rural Cycle

The three controllers have similar performance in the RDE Rural cycle, although A-ECMS tends to use the electric motor and charge the battery after the SOC is in the lower limit, there is not too much chance for the electric motor to power the vehicle in RDE Rural cycle.

Thereby, due to the fewer occasions of using the electric motor, the fuel consumption gap between DP and A-ECMS is smaller than the RDE Urban driving cycle.

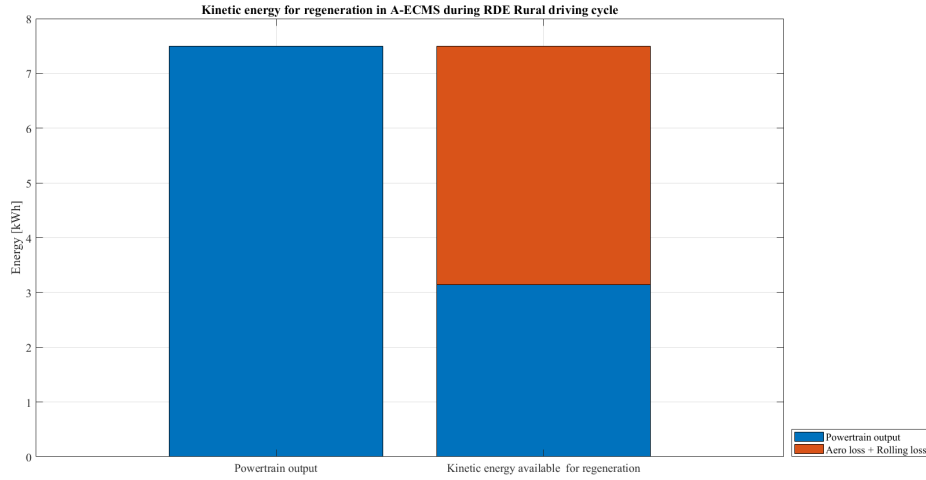


Figure 4.32: P1 48V Kinetic energy in A-ECMS during RDE Rural driving cycle

4.4 P1 48V architecture in the RDE Motorway Cycle

The RDE Motorway cycle is also down-scaled due to the limited performance of the vehicle. However, It still tests the vehicle in a high-speed condition. In the RDE Motorway driving cycle, the distributions of engine operation points for these two algorithms are similar in terms of BSFC (shown in Figure 4.33), resulting in little fuel consumption difference between these two algorithms. Furthermore, Table 4.10 shows that the performances of these three s-factor controllers are very close.

Table 4.10: P1 48V architecture performance - RDE Motorway

Performance - RDE Motorway	DynaProg	A-ECMS	Relay	PID
Fuel consumption [L]	3.165	3.344	3.340	3.351
Fuel consumption gap	Reference	+5.656%	+5.529%	+5.877%
SOC variation [%]	-0.348%	+4.423%	0.491%	+5.027%

4.4.1 Comparison of power flows and torque of ICE with DP and A-ECMS

When it comes to the power flow of ICE (Figure 4.34), the power flows of ICE with the two algorithms are almost the same, and DP still has a higher torque profile, which makes the engine operating points closer to OOL.

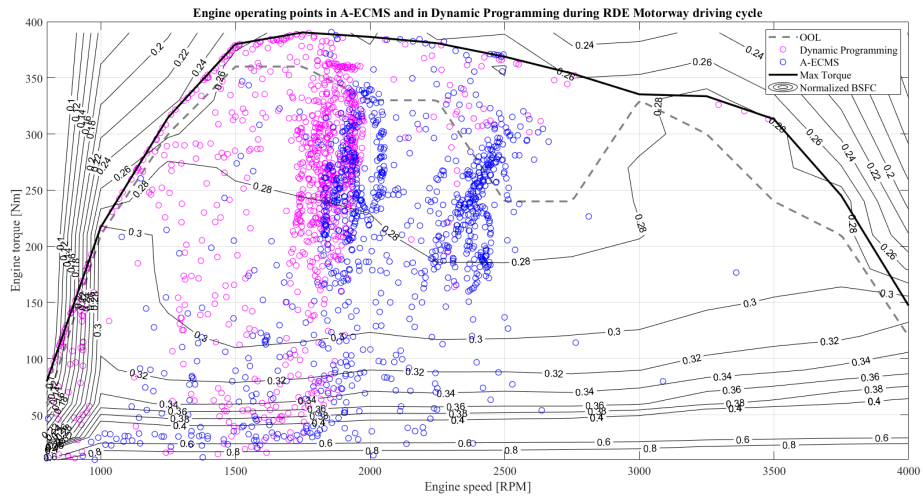


Figure 4.33: P1 48V Engine operating points of DP and A-ECMS during the RDE Motorway driving cycle

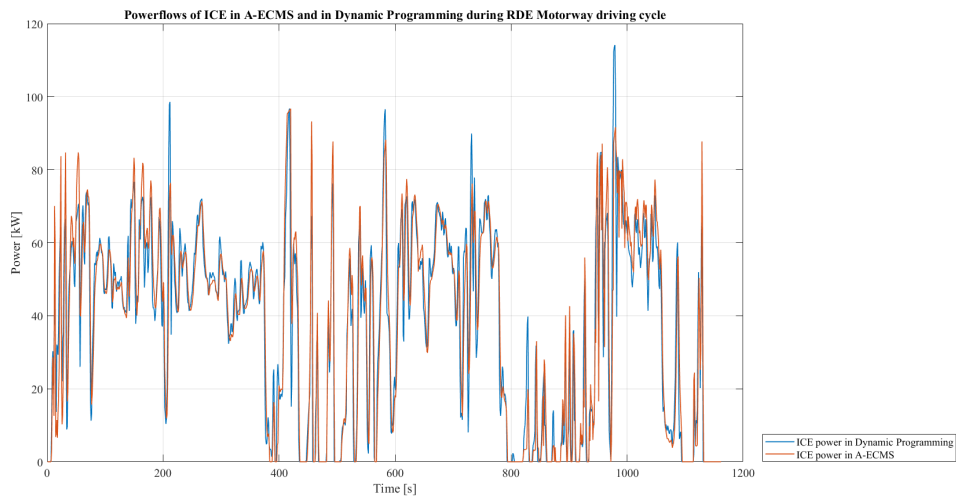


Figure 4.34: P1 48V Power flows of ICE in DP and A-ECMS during the RDE Motorway driving cycle

4.4.2 Comparison of power flows and torque of the electric motor with DP and A-ECMS

Similar to previous cycles, DP has lower electric motor power but higher electric motor torque, and the comparison is plotted in Figure 4.35. It is obvious that the

occasions of using the electric motor are even fewer than those in the RDE Rural cycle because of the high-speed characteristics of the RDE Motorway cycle.

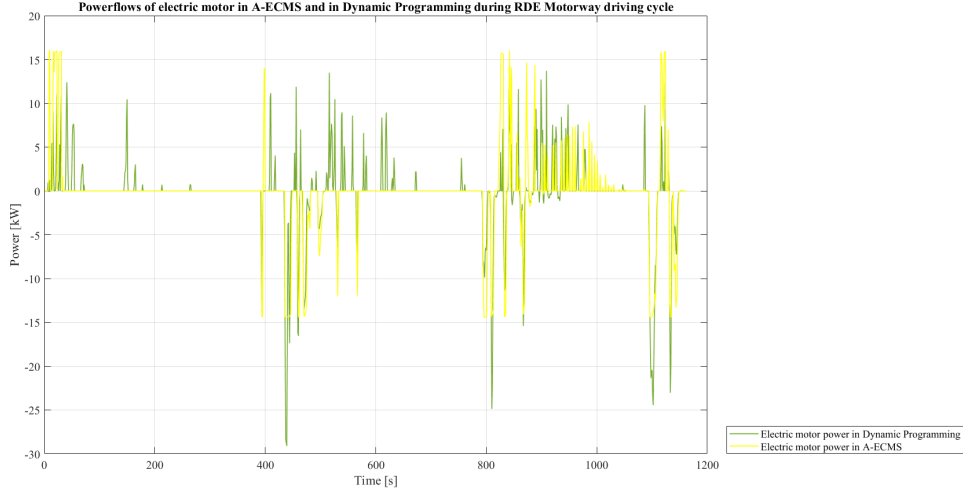


Figure 4.35: P1 48V Power flows of the electric motor in DP and A-ECMS during the RDE Motorway driving cycle

4.4.3 Comparison of SOC with DP and A-ECMS

Figure 4.36 compares the SOC variation of the DP algorithm and the ECMS algorithm with three different Equivalence Factor controllers during the RDE Motorway driving cycle, respectively. A-ECMS and DP tend to use the electric motor at the beginning of the driving cycle, and there are not so many opportunities for the electric motor to power the vehicle at high speeds. The PID controller and Relay-based switching logic still do not use the electric motor from the start of the driving cycle. The sharp braking in the driving cycle renders more energy regeneration that results in a higher SOC at the end of the driving cycle for all s-factor controllers.

4.4.4 Comparison of fuel consumption with DP and A-ECMS

Figure 4.37 illustrates the accumulation curve of fuel consumption of the DP and the ECMS algorithm with three different Equivalence Factor controllers during the RDE Motorway driving cycle, respectively. The 3 controllers have very similar fuel consumption and are rather close to the DP because, in the RDE Motorway

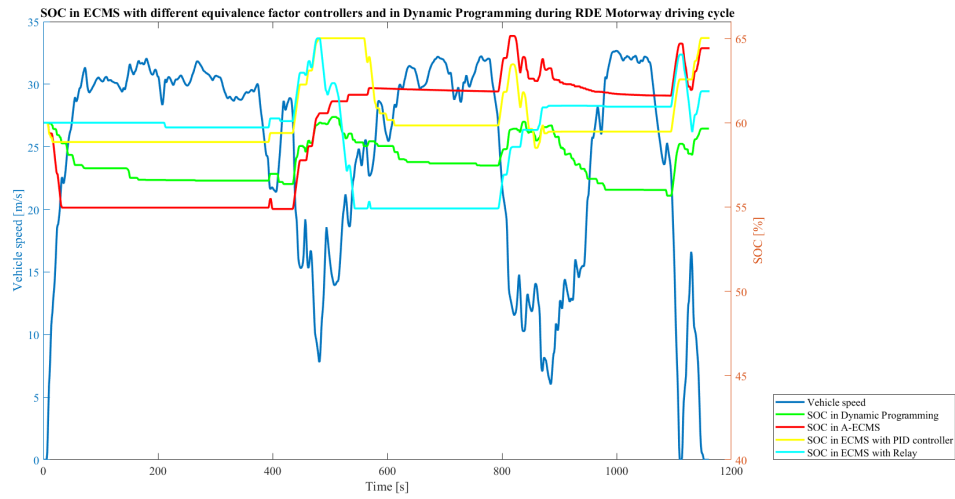


Figure 4.36: P1 48V SOC in DP and A-ECMS during the RDE Motorway driving cycle

driving cycle, only a little energy can be provided by the electric motor due to the high-speed characteristics of the driving cycle.

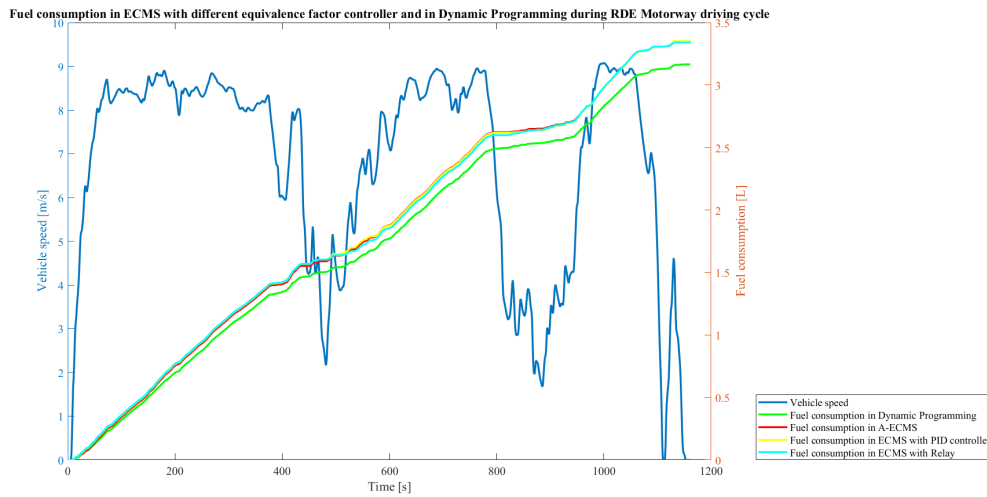


Figure 4.37: P1 48V Fuel consumption in DP and A-ECMS during the RDE Motorway driving cycle

4.4.5 Energy contribution and loss with A-ECMS

As it is observed in Figure 4.38, only 2% of energy is provided by the electric motor because it is impossible for the electric motor to engage the power generation in high-speed conditions due to its limited power. Figure 4.39 shows that the majority of loss is from aerodynamics (60%) because of the high-speed characteristics of the driving cycle. The driveline loss and rolling loss are 13% and 18%, respectively. The detailed data about the energy and loss are listed in Table 4.11 and Table 4.12.

Table 4.11: P1 48V architecture Energy contribution in RDE Motorway driving cycle

Energy - RDE Motorway [kWh]	DynaProg	A-ECMS	Relay	PID
Energy delivered by ICE	11.721	12.435	12.420	12.469
Energy delivered by electric motor	0.189	0.193	0.228	0.173
Energy delivered by powertrain	11.899	12.628	12.647	12.642
Regenerative energy	-0.227	-0.324	-0.301	-0.310

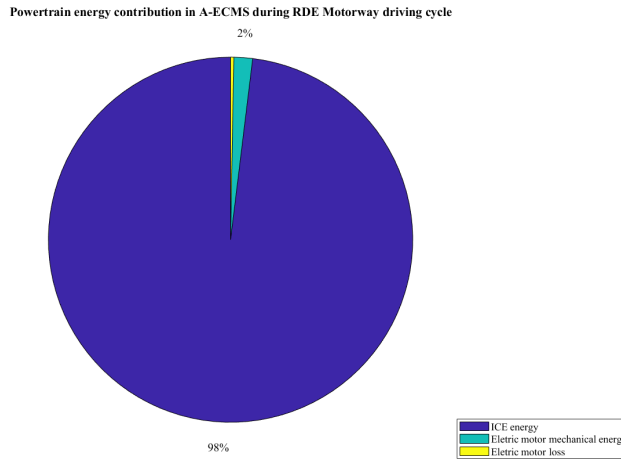


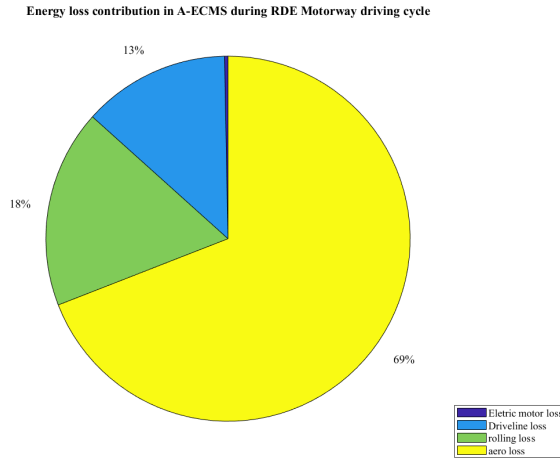
Figure 4.38: P1 48V Energy contribution in A-ECMS during the RDE Motorway driving cycle

4.4.6 Available regenerative energy in A-ECMS algorithm

Only a few of kinetic energy can be reused theoretically. On account of the high aerodynamic resistance in high-speed conditions, as Figure 4.40 shows. These

Table 4.12: P1 48V architecture Energy loss in RDE Motorway driving cycle

Energy Losses in RDE Motorway [kWh]	DynaProg	A-ECMS	Relay	PID
Aerodynamic loss	7.867	7.826	7.825	7.826
Rolling loss	2.687	2.140	2.140	2.141
Electric loss	0.027	0.037	0.037	0.034
Driveline loss	0.596	1.837	1.858	1.871

**Figure 4.39:** P1 48V Energy loss in A-ECMS during the RDE Motorway driving cycle

phenomena of the available regenerative energy change with the speed are consistent with the literature [25], which demonstrates that the available energy for regeneration is higher in urban or low-speed conditions but lower in high-speed conditions.

4.4.7 Summary of P1 48V architecture with DP and ECMS in the RDE Motorway Cycle

In the RDE Motorway driving cycle, the electric motor does not frequently participate in the energy supply at high speeds, so these three s-factor controllers perform similarly and cannot further explore the potential of the electric motor. And their performances are very close to the performance of DP.

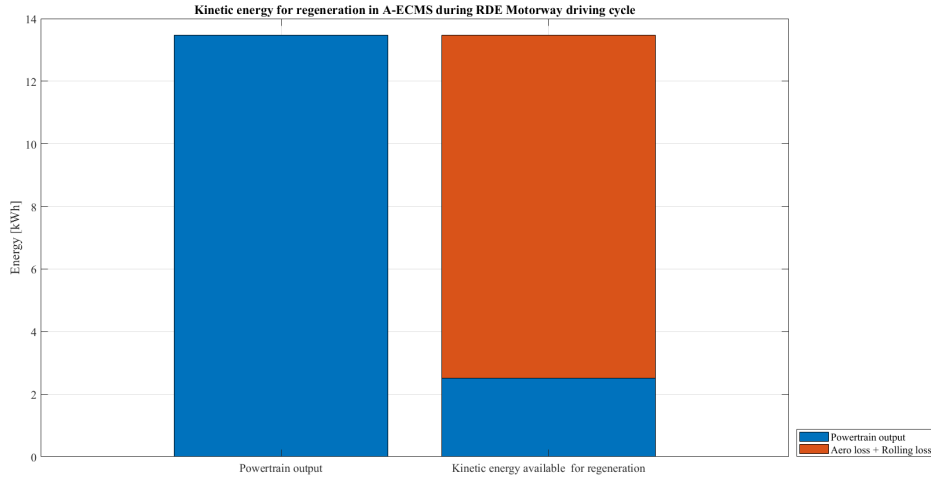


Figure 4.40: P1 48V Kinetic energy in A-ECMS during the RDE Motorway driving cycle

4.5 P1 48V architecture vs. P2 200V architecture electric motor

Table 4.13: Performance of P1 (CS) and P2 (CS with double-sized battery) compared to Pure ICE mode

Architecture	ICE-only	P1 (CS)	P2 (CS 2xBat.)
Fuel consumption [L]	2.456	2.263	2.105
Fuel consumption gap	Reference	-7.858%	-14.292%
SOC variation [%]	-	0	0

Under identical ICE specifications, the P1 architecture (Figure 3.1) integrates a 48V motor, and the P2 architecture (Figure P2 3.8) is generally equipped with a 200V motor, with clutches that allow for pure electric operating mode. For consistency of the efficiency of the electric motor, we still use the map of a 48V motor but a double-sized battery to mimic the 200V motor. By using the DP algorithm, it can be observed that the P2 architecture can further reduce fuel consumption by 6.434% compared to the P1 architecture with the same charge-sustaining (CS) strategy due to its flexibility in selecting operating modes, allowing the engine to operate in more efficient areas of the engine map. However, the complexity of P2 architecture makes this increase in fuel economy less worthwhile.

4.5.1 P1 charge-sustaining vs. P2 charge-sustaining

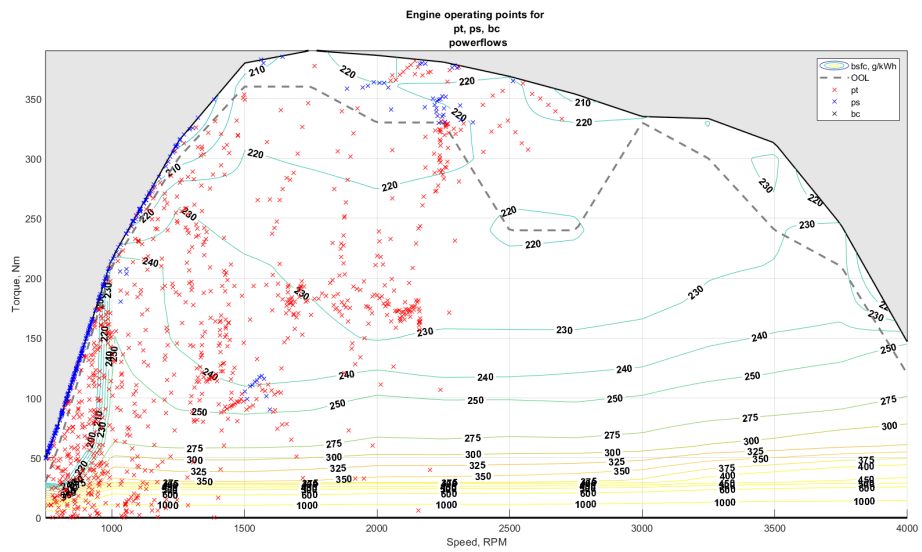


Figure 4.41: P1 48V architecture Engine operating map (charge-sustaining)

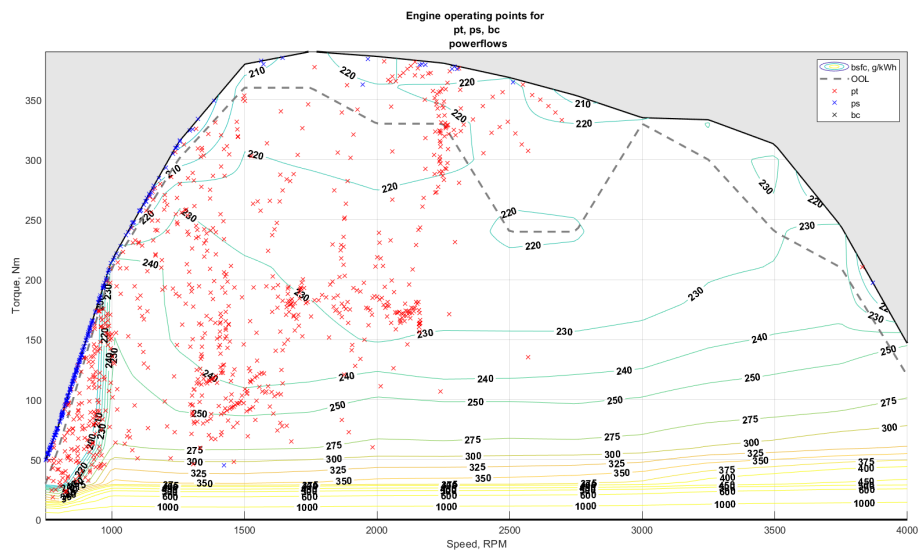


Figure 4.42: P2 200V architecture Engine operating map (charge-sustaining)

Figure 4.41 and Figure 4.42 are the engine operating maps for P1 and P2 (with double-sized battery) architectures with CS strategy, respectively. The red points

refer to pure ICE mode, and the blue points represent power-split mode. It can be seen that in the P2 architecture, there are fewer operating points located in the high BSFC region. However, we found the gap in fuel consumption between P1 and P2 is only 6.434% (see Table 4.13) because we have very stringent constraints of the final SOC and SOC window. What if we reduce the limitation of SOC by using a charge-depleting strategy (CD)?

4.5.2 P1 charge-sustaining vs. P2 charge-depleting

Table 4.14: Performance of P1 (CS) and P2 (CD with double-sized battery) compared to Pure ICE mode

Architecture	ICE-only	P1 (CS)	P2 (CD 2xBat.)
Fuel consumption [L]	2.456	2.263	1.618
Fuel consumption gap	Reference	-7.858%	-34.121%
SOC variation [%]	-	0	-60.0%

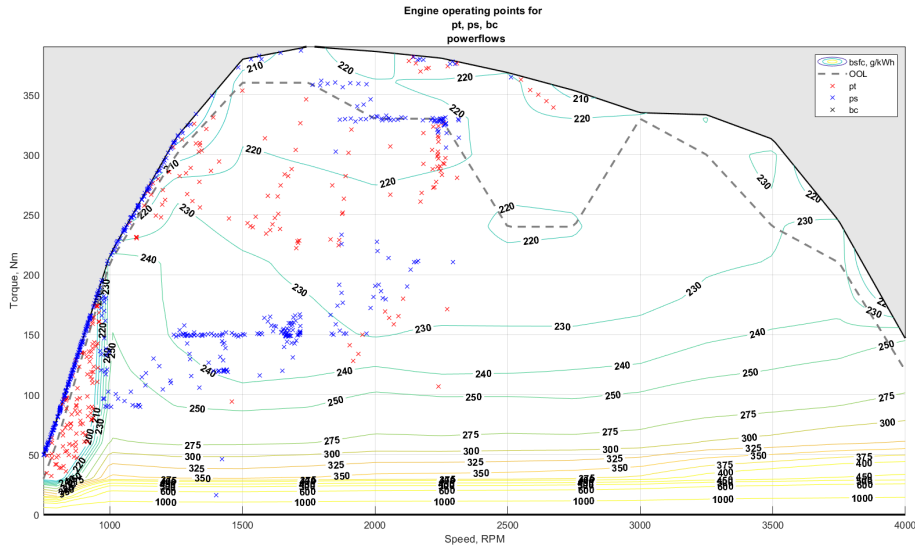


Figure 4.43: P2 200V architecture Engine operating map (charge-depleting)

When the strict SOC constraints are relieved (namely, the CD strategy), the engine map (Figure 4.43) shows a large number of power-split mode points that are very close to the optimal operating line (OOL), significantly reducing fuel consumption. While, it should be noted that due to limitations of battery performance, these points are not realistic.

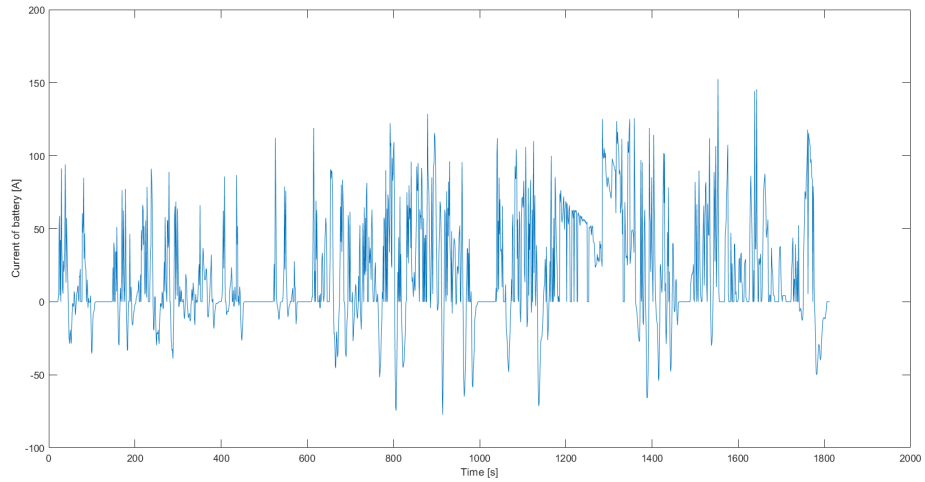


Figure 4.44: P2 200V architecture battery current (charge-depleting)

Operating the P2 architecture (with double-sized battery) with a CD strategy, the fuel consumption can be further decreased by 26.263% compared to the P1 architecture with CS strategy (shown in Table 4.14). However, for safety and sustainability reasons, overly frequent battery charging and discharging in this case (Figure 4.44) is not feasible in reality.

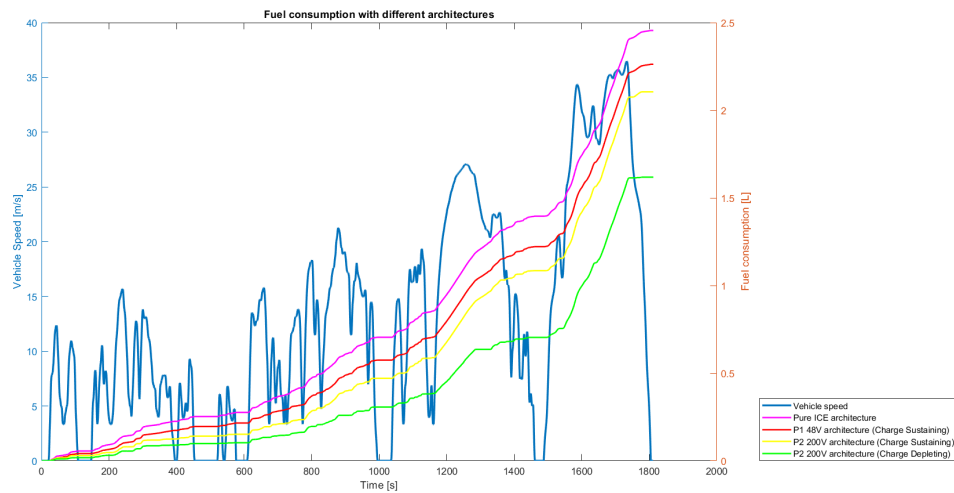


Figure 4.45: Fuel consumption with different architectures

In summary, as Figure 4.45 illustrates, the P2 architecture shows the ability

to reduce additional fuel consumption by approximately 6.434% when using the same CS strategy. However, the complex structure of the P2 architecture leads to higher production costs and potentially reduced reliability. Additionally, the P2 architecture with the CD strategy can significantly decrease fuel consumption by about 26.263% even further. By integrating all the results above, it can be concluded that the P1 48V architecture is the most suitable configuration for the IVECO DAILY since it can provide satisfactory performance with acceptable complexity and sustainability.

4.6 P1 48V architecture with different battery sizes

As depicted in Table 4.15, under the P1 48V architecture, there is a noticeable reduction in fuel consumption as the battery size increases, from 2.262L with 0.5kWh to 2.208L with 1.5kWh, which is about -2.387%. However, the effect of excessive battery size exceeding 1.5kWh can be ignored. Figure 4.46 graphically shows the fuel consumption with different battery sizes.

Table 4.15: Performance of P1 48V architecture with different battery size

Battery size [kWh]	Fuel consumption [L]	SOC variation [%]
ICE-only	2.456	-
0.5	2.262	+0.528%
0.75	2.230	+0.160%
1	2.219	+0.119%
1.5	2.208	-0.015%
2	2.207	-0.028%
3	2.207	-0.041%

Figure 4.47 illustrates the comparison of SOC with varying battery sizes. The observation is clear: a larger battery size leads to a more stable SOC change. This is because, with a larger battery, the same energy consumption represents a smaller proportion of the total energy, resulting in a smaller SOC change.

Overall, 1.5kWh is the most appropriate battery size for P1 48V architecture, which reduces the fuel consumption by over 2% compared to the 0.5kWh battery. And no further benefit is derived from overly large battery sizes.

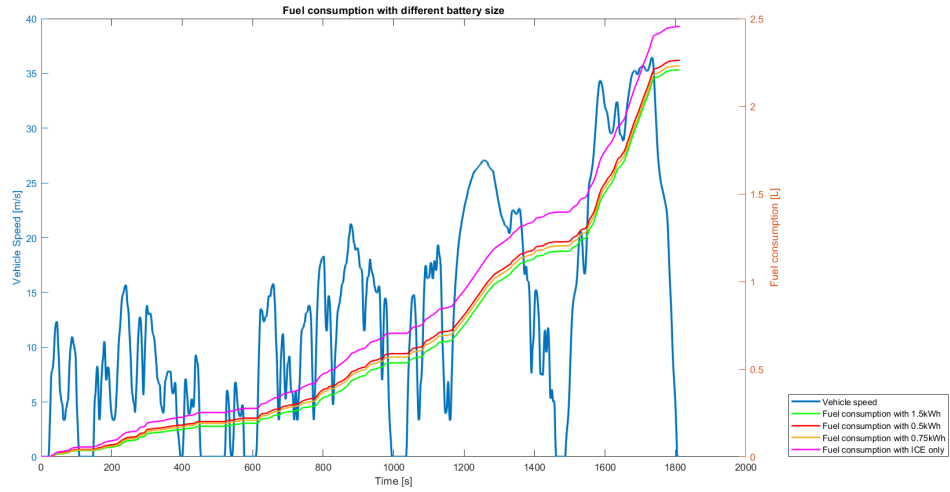


Figure 4.46: P1 48V Fuel consumption with different battery size

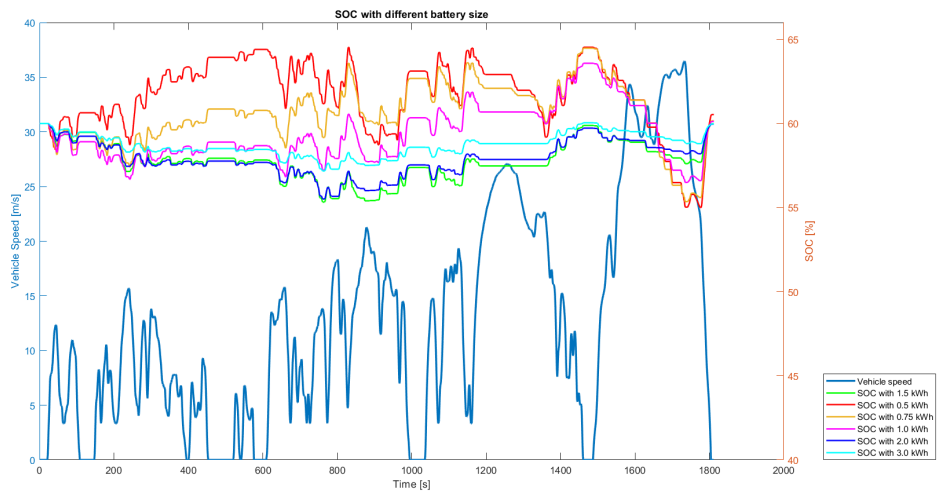


Figure 4.47: P1 48V SOC variation with different battery sizes

Chapter 5

Summary of thesis and future works

5.1 Summary

In the configuration of P1 48V architecture, DP enables the engine to operate in areas with low BSFC, close to OOL, thereby reducing fuel consumption. The gap in fuel consumption between DP and ECMS is 2.659% to 5.610% depending on different driving cycles. However, DP is a backward approach that may not be practically implementable. Nevertheless, the solutions derived from DP serve as valuable references.

Table 5.1: Coast-down values in Simulation

Vehicle mass	2620 kg
F0	345 N
F1	0 N/(km/h)
F2	0.1007 N/(km/h) ²

When using the fuel consumption of the forward model with ICE-only mode over the WLTC and RDE driving cycles as a reference and considering the results of DP as the theoretical optimum (shown in Table 5.2), the A-ECMS controller demonstrates potential, particularly in the RDE Urban driving cycle, where low speeds allow for increased electric motor engagement. The A-ECMS controller efficiently utilizes the battery from the start, maintaining charging sustainability by smoothly adjusting the s-factor based on SOC variation, thereby controlling the use of an electric motor. The fuel consumption gap between A-ECMS and DP is 4.528% in the RDE Urban driving cycle, while that for the Relay-based controller is

Table 5.2: Fuel consumption gap between Pure-ICE mode and various HEV algorithms during WLTC and RDE driving cycles

P1 48V	ICE-only	DP	A-ECMS	Relay	PID
WLTC [L]	2.482	2.263	2.329	2.335	2.345
FC gap	Reference	-8.823%	-6.164%	-5.923%	-5.520%
R. Urban [L]	0.832	0.657	0.703	0.712	0.705
FC gap	Reference	-20.033%	-15.505%	-14.423%	-15.264%
R. Rural [L]	2.120	1.910	2.016	2.012	2.009
FC gap	Reference	-9.906%	-4.906%	-5.094%	-5.235%
R. Motorway [L]	3.363	3.165	3.344	3.340	3.351
FC gap	Reference	-5.888%	-0.565%	-0.684%	-0.357%

5.610%, the extra benefit of fuel economy due to the A-ECMS is over 1%. On the other hand, the PID controller is robust, tightly controlling SOC around the target value, beneficial for extending battery life. However, overly aggressive variations in the s-factor can impact fuel consumption and battery life. Differences among these s-factor controllers tend to diminish during high-speed driving cycles, where electric motor utilization is limited.

What is worth mentioning is that A-ECMS and the PID controller have nearly 5% SOC increase at the end of the RDE Motorway driving cycle, which means that the electrical energy stored after this driving cycle can be used to save future fuel consumption[26].

Table 5.3: Fuel consumption gap of different HEV architecture during the WLTC driving cycle

Architecture	ICE-only	P1 (CS)	P2 (CS 2xBat.)	P2 (CD 2xBat.)
Fuel consumption [L]	2.456	2.263	2.105	1.618
Fuel consumption gap	Reference	-7.858%	-14.292%	-34.121%
SOC variation [%]	-	0	0	-60.0%

Regarding different HEV architectures (Table 5.3), the P2 architecture offers greater power-split flexibility but also increases complexity, and fuel economy only further improves by 6.434% compared to the P1 architecture. Unless the charge-depleting strategy can be used, P1 48V is the best choice to balance complexity and performance.

Battery selection is more straightforward (Table 5.4), with higher capacity resulting in lower fuel consumption, where the fuel consumption decreases over 2% when changing the battery size from 0.5kWh to 1.5kWh, but exceeding capacity does not bring further advantages. Therefore, 1.5kWh is the most suitable solution.

Table 5.4: Fuel consumption gap with different battery sizes during the WLTC driving cycle

Battery size [kWh]	Fuel consumption gap
ICE-only	Reference
0.5	-7.899%
1.5	-10.098%
3	-10.138%

In conclusion, from the software perspective, the A-ECMS shows promising potential in urban conditions, effectively exploiting the motor while maintaining charge sustainability. The PID controller in ECMS robustly maintains the SOC around the target value. The Relay-based controller efficiently manages the s-factor with a simple structure. The ECMS has closely approximated DP with a fuel consumption gap of less than 6% when the s-factor is effectively controlled. However, A-ECMS and PID controllers are not yet optimized to their full potential due to finite time and can be further refined. From the hardware viewpoint, the P1 48V architecture shows satisfactory results with less complexity compared to the P2 200V architecture. The optimal battery size for the P1 48V architecture is determined to be 1.54 kWh.

5.2 Future works

The possible future works for the A-ECMS and the PID controller include further tuning in parameters, such as gain and sampling rate, and the refinement of the architecture. For instance, what is very interesting is that the performance of A-ECMS varies with driving scenarios. Is it possible to associate the s-factor with the vehicle speed and acceleration? If so, the electric motor might be further used at low speeds and frequent acceleration and deceleration conditions to prevent less efficient ICE operations. On the contrary, the electric motor might be shut down during high-speed conditions to save electricity.

As for DP, although the optimal trajectory obtained from it cannot be directly implemented, the results can be used to design a rule-based controller that is simple to utilize. In addition, is it possible to leverage machine learning tools such as Clustering-Optimized Rule-Extraction (CORE)[27] to extract some rules from the DP results? This CORE provides a way to convert the optimal theory into actionable control strategies.

Finally, regarding the P2 200V architecture, its flexibility and complexity bring challenges and opportunities. Identifying an appropriate automotive product that can effectively utilize this architecture is a possible further step. It includes

evaluating specific vehicle models or applications where the P2 200V architecture can maximize its advantages and reduce the impact of its complexity.

List of Tables

2.1	Tuning of SOC window	15
2.2	Tuning of target SOC	15
2.3	Performance of different proportional gain c_p	16
2.4	Performance of different time intervals for sampling	17
2.5	Performance of different initial s-factor	18
3.1	IVECO DAILY specification	19
3.2	Coast-down values in Model Validation	26
3.3	ICE-only results - WLTC	27
3.4	Model mismatch - WLTC	27
3.5	ICE-only results - RDE	27
3.6	Model mismatch - RDE	29
4.1	P1 48V architecture performance - WLTC	35
4.2	P1 48V architecture Energy contribution in WLTC driving cycle	41
4.3	P1 48V architecture Energy loss in WLTC driving cycle	43
4.4	P1 48V architecture performance - RDE Urban	45
4.5	P1 48V architecture Energy contribution in RDE Urban driving cycle	48
4.6	P1 48V architecture Energy loss in RDE Urban driving cycle	50
4.7	P1 48V architecture performance - RDE Rural	51
4.8	P1 48V architecture Energy contribution in RDE Rural driving cycle	55
4.9	P1 48V architecture Energy loss in RDE Rural driving cycle	56
4.10	P1 48V architecture performance - RDE Motorway	57
4.11	P1 48V architecture Energy contribution in RDE Motorway driving cycle	61
4.12	P1 48V architecture Energy loss in RDE Motorway driving cycle	62
4.13	Performance of P1 (CS) and P2 (CS with double-sized battery) compared to Pure ICE mode	63
4.14	Performance of P1 (CS) and P2 (CD with double-sized battery) compared to Pure ICE mode	65
4.15	Performance of P1 48V architecture with different battery size	67

5.1	Coast-down values in Simulation	69
5.2	Fuel consumption gap between Pure-ICE mode and various HEV algorithms during WLTC and RDE driving cycles	70
5.3	Fuel consumption gap of different HEV architecture during the WLTC driving cycle	70
5.4	Fuel consumption gap with different battery sizes during the WLTC driving cycle	71

List of Figures

1.1	Global EV market projection between 2021 and 2026	2
1.2	PITEF Project	3
1.3	IVECO DAILY	5
2.1	HEVs control tasks, where ECU is the Engine Control Unit, TCU is the Transmission Control Unit, BMS is the Battery Management System, and MCU is the Motor Control Unit	10
2.2	Adaptive ECMS controller architecture	16
2.3	Tuning of proportional gain c_p	17
2.4	Tuning of time intervals for sampling	18
2.5	Tuning of initial s-factor	18
3.1	P1 architecture	20
3.2	Simplified battery model	22
3.3	Battery specification	23
3.4	Forward modeling approach	25
3.5	Backward modeling approach	26
3.6	Engine operating points for ECMS, DP, and Real Experiment in Pure ICE mode during WLTC driving cycle	28
3.7	Gear number in ECMS, in DP and in Real Experiment, with Pure ICE mode during WLTC driving cycle	28
3.8	P2 architecture	31
4.1	P1 48V Main profile with DP in WLTC	33
4.2	P1 48V Power profile with DP in WLTC	34
4.3	P1 48V Engine operating points of DP and A-ECMS during WLTC driving cycle	35
4.4	P1 48V Power flows of ICE in A-ECMS and DP during WLTC driving cycle	36
4.5	P1 48V Torque of ICE in A-ECMS and DP during WLTC driving cycle	37

4.6 P1 48V Gear numbers in A-ECMS and DP during WLTC driving cycle	37
4.7 P1 48V Power flows of electric motor in A-ECMS and DP during WLTC driving cycle	38
4.8 P1 48V Torque of electric motor in A-ECMS and DP during WLTC driving cycle	39
4.9 P1 48V Fuel consumption in A-ECMS and DP during WLTC driving cycle	39
4.10 P1 48V SOC variation in A-ECMS and DP during WLTC driving cycle	40
4.11 P1 48V Energy contribution in DP during WLTC driving cycle . . .	42
4.12 P1 48V Energy contribution in A-ECMS during WLTC driving cycle	42
4.13 P1 48V Energy loss in DP during WLTC driving cycle	43
4.14 P1 48V Energy loss in A-ECMS during WLTC driving cycle	44
4.15 P1 48V Kinetic energy in DP during WLTC driving cycle	44
4.16 P1 48V Kinetic energy in A-ECMS during WLTC driving cycle . .	45
4.17 P1 48V Engine operating points of DP and A-ECMS during RDE Urban driving cycle	46
4.18 P1 48V Power flows of ICE in DP and A-ECMS during RDE Urban driving cycle	47
4.19 P1 48V Power flows of the electric motor in DP and A-ECMS during RDE Urban driving cycle	47
4.20 P1 48V SOC in DP and A-ECMS during RDE Urban driving cycle	48
4.21 P1 48V Fuel consumption in DP and A-ECMS during RDE Urban driving cycle	49
4.22 P1 48V Energy contribution in A-ECMS during RDE Urban driving cycle	49
4.23 P1 48V Energy loss in A-ECMS during RDE Urban driving cycle .	50
4.24 P1 48V Kinetic energy in A-ECMS during RDE Urban driving cycle	51
4.25 P1 48V Engine operating points of DP and A-ECMS during RDE Rural driving cycle	52
4.26 P1 48V Power flows of ICE in DP and A-ECMS during RDE Rural driving cycle	53
4.27 P1 48V Power flows of the electric motor in DP and A-ECMS during RDE Rural driving cycle	53
4.28 P1 48V SOC in DP and A-ECMS during RDE Rural driving cycle .	54
4.29 P1 48V Fuel consumption in DP and A-ECMS during RDE Rural driving cycle	54
4.30 P1 48V Energy contribution in A-ECMS during RDE Rural driving cycle	55
4.31 P1 48V Energy loss in A-ECMS during RDE Rural driving cycle . .	56

4.32 P1 48V Kinetic energy in A-ECMS during RDE Rural driving cycle	57
4.33 P1 48V Engine operating points of DP and A-ECMS during the RDE Motorway driving cycle	58
4.34 P1 48V Power flows of ICE in DP and A-ECMS during the RDE Motorway driving cycle	58
4.35 P1 48V Power flows of the electric motor in DP and A-ECMS during the RDE Motorway driving cycle	59
4.36 P1 48V SOC in DP and A-ECMS during the RDE Motorway driving cycle	60
4.37 P1 48V Fuel consumption in DP and A-ECMS during the RDE Motorway driving cycle	60
4.38 P1 48V Energy contribution in A-ECMS during the RDE Motorway driving cycle	61
4.39 P1 48V Energy loss in A-ECMS during the RDE Motorway driving cycle	62
4.40 P1 48V Kinetic energy in A-ECMS during the RDE Motorway driving cycle	63
4.41 P1 48V architecture Engine operating map (charge-sustaining) . . .	64
4.42 P2 200V architecture Engine operating map (charge-sustaining) . .	64
4.43 P2 200V architecture Engine operating map (charge-depleting) . . .	65
4.44 P2 200V architecture battery current (charge-depleting)	66
4.45 Fuel consumption with different architectures	66
4.46 P1 48V Fuel consumption with different battery size	68
4.47 P1 48V SOC variation with different battery sizes	68

Bibliography

- [1] *Global EV market projection between 2021 and 2026*. URL: <https://www.statista.com/statistics/1334673/global-electric-vehicle-market-forecast-by-type/>. (accessed: 07.11.2023) (cit. on p. 1).
- [2] C.C. Chan. *The state of the art of electric and hybrid vehicles*. *Proc. IEEE* 90(2). 2002 (cit. on p. 1).
- [3] L. Guzzella, A. Sciarretta. *Vehicle Propulsion Systems: Introduction to Modeling and Optimization*. 2013 (cit. on p. 2).
- [4] *Piattaforma tecnologica di Filiera Pi.Te.F.* URL: <https://www.regione.piemonte.it/web/temi/fondi-progetti-europei/fondo-europeo-sviluppo-regionale-fesr/programmazione-2014-2020/piattaforma-tecnologica-filiera-pitef>. (accessed: 25.06.2023) (cit. on p. 3).
- [5] A.A. Pesaran. *Choices and requirements of batteries for EVs, HEV, PHEV*. NREL/PR-5400-51474. 2011 (cit. on p. 6).
- [6] J.M. Miller. «Propulsion Systems for Hybrid Vehicles». In: *The Institution of Electrical Engineers* (2003) (cit. on p. 8).
- [7] S. Onori et al. «Hybrid Electric Vehicles, Springer Briefs in Control, Automation and Robotics». In: (2015). DOI: 10.1007/978-1-4471-6781-5_3 (cit. on p. 9).
- [8] L. Guzzella A. Sciarretta. «Control of hybrid electric vehicles.» In: *IEEE Control Syst. Mag.* 27(2) (2007), pp. 60–70 (cit. on p. 9).
- [9] F. Salmasi. «Control strategies for hybrid electric vehicles: evolution, classification, comparison, and future trends.» In: *IEEE Trans. Veh. Technol.* 56(5) (2007), pp. 2393–2404 (cit. on p. 9).
- [10] S. Onori. «Model-Based Optimal Energy Management Strategies for Hybrid Electric Vehicles». In: *Lecture Notes in Control and Information Sciences*, vol. 455 (Springer, New York) (2014), pp. 199–218 (cit. on p. 9).
- [11] B. Baumann G. Washington B. Glenn G. Rizzoni. «Mechatronic design and control of hybrid electric vehicles». In: *IEEE/ASME Trans. Mechatron.* 5(1) (2000), pp. 58–72 (cit. on p. 9).

- [12] C. Lin J. Kang J. Grizzle H. Peng. «Energy management strategy for a parallel hybrid electric truck». In: *Proceedings of the 2001 American Control Conference, vol. 4 (2001)* (2001), pp. 2878–2883 (cit. on p. 9).
- [13] D. Bianchi L. Rolando L. Serrao S. Onori G. Rizzoni N. Al-Khayat T.M. Hsieh P. Kang. «Layered control strategies for hybrid electric vehicles based on optimal control». In: *Int. J. Electr. Hybrid Veh. 3(2)* (2011), pp. 191–217 (cit. on p. 9).
- [14] D. Bertsekas. *Dynamic Programming and Optimal Control (Athena Scientific)*. Belmont, 1995 (cit. on pp. 9, 10).
- [15] A. Piccolo L. Ippolito V. Galdi A. Vaccaro. «Optimization of energy flow management in hybrid electric vehicles via genetic algorithms». In: *Proceedings of the 2001 IEEE/ASME International Conference on Advanced Intelligent Mechatronics*. 2001 (cit. on p. 10).
- [16] H.P. Geering. *Optimal Control with Engineering Applications*. Berlin: Springer, 2007 (cit. on p. 11).
- [17] Giorgio Rizzoni Simona Onori Lorenzo Serrao. «Adaptive Equivalent Consumption Minimization Strategy for Hybrid Electric Vehicles». In: *Proceedings of the ASME 2010 Dynamic Systems and Control Conference*. 2010 (cit. on p. 11).
- [18] Bellman, R.E. *Optimal Control with Engineering Applications*. ISBN 0-486-42809-5. Dover, 2003 (cit. on p. 11).
- [19] Ezio Spessa Federico Miretti Daniela Misul. «DynaProg: Deterministic Dynamic Programming solver for finite horizon multi-stage decision problems». In: *SoftwareX* Volume 14 (2021). DOI: <https://doi.org/10.1016/j.softx.2021.100690> (cit. on p. 12).
- [20] *Dynamic Programming Toolbox link*. URL: <https://github.com/fmiretti/DynaProg>. (accessed: 21.11.2023) (cit. on p. 12).
- [21] Feng J. Li M. and Han Z. «Improved Energy Management with Vehicle Speed and Weight Recognition for Hybrid Commercial Vehicles». In: *SAE Technical Paper* (2022). DOI: [10.4271/2022-01-7052](https://doi.org/10.4271/2022-01-7052) (cit. on pp. 13, 15).
- [22] Dirk Uwe Sauer T. Bank S. Klamor N. Löffler. «Performance benchmark of state-of-the-art high-power lithium-ion cells and implications for their usability in low-voltage applications». In: *Journal of Energy Storage* 36 (2021). DOI: <https://doi.org/10.1016/j.est.2021.102383> (cit. on p. 22).
- [23] MIT Electric Vehicle Team. «A Guide to Understanding Battery Specifications». In: (2008) (cit. on p. 22).
- [24] Giorgio Rizzoni Simona Onori Lorenzo Serrao. «Hybrid Electric Vehicles Energy Management». In: (), p. 15 (cit. on p. 43).

BIBLIOGRAPHY

- [25] Giorgio Rizzoni Simona Onori Lorenzo Serrao. «Hybrid Electric Vehicles Energy Management». In: (), p. 17 (cit. on p. 62).
- [26] Giorgio Rizzoni Simona Onori Lorenzo Serrao. «Hybrid Electric Vehicles Energy Management». In: (), pp. 65–67 (cit. on p. 70).
- [27] *Cluster analysis*. URL: https://en.wikipedia.org/wiki/Cluster_analysis. (accessed: 22.11.2023) (cit. on p. 71).